Forensic Chemistry 44 (2025) 100663

Contents lists available at ScienceDirect

Forensic Chemistry

journal homepage: www.sciencedirect.com/journal/forensic-chemistry

Electrodeposition of redox materials with potential for enhanced visualisation of latent finger-marks on brass substrates and ammunition casings.

Colm McKeever, Eithne Dempsey *

Department of Chemistry, Kathleen Lonsdale Institute for Human Health Research, Maynooth University, Maynooth, County Kildare, W23 DD4R, Ireland.

ARTICLE INFO

Keywords:
Electrodeposition
Latent finger-marks
Visualising process
Phenothiazines
Brass
Ammunition casings

ABSTRACT

Electrochemical methods can play a key role in the analysis of impression evidence, specifically, latent finger-marks on brass substrates and ammunition casings, the latter being commonly encountered at crime scenes in forensic casework. In adopting such techniques, forensic investigators can potentially overcome some of the challenges associated with traditional visualisation methods, the use of aggressive reagents, preservation of evidence integrity and the need for extensive sample preparation. The spatially selective deposition of conducting/redox active polymers for visualising latent finger-marks on typically low-yield brass ammunition casings is examined here, exploiting the electrodeposition of 3,4-ethylenedioxythiophene (EDOT), together with a first-time study of phenozine vs. phenothiazine monomers, and their combinations at sheet and cartridge brass. Fine tuning of electrochemical protocols and conditions together with optimised monomer feedstocks played a key role in the finger-mark visualisation quality achieved with insights into brass electrochemistry. EDOT-thionine emerged consistently as the most effective combination upon electrochemical deposition on brass sheets, revealing latent finger-marks (groomed) at the highest level of detail (level 3), including pores within the papillary ridges, using a low energy, rapid (t = 120 s) constant potential (E_{app} = 0.1 V vs Ag|AgCl) approach. Successful visualisation of groomed and natural (donor) latent finger-marks was achieved following exposure of brass to temperatures of 700 °C and > 15-month room temperature aging. Bespoke electrochemical cells designed to facilitate the use of ammunition casings as working electrodes produced excellent results via potential sweeping, resulting in pristine visualised latent finger-marks (groomed) of grade 3 quality with visible level 3 (> 50 %) features.

1. Introduction

Latent finger-marks arise from natural secretions of the skin (produced by eccrine and sebaceous glands) remaining on a surface following contact. Eccrine sweat is ca. 98 % water, containing inorganic (chlorides, ammonias, phosphates) and organic (amino acids, urea, sugars) species, while residue from sebaceous glands contains mostly organic compounds (glycerides, fatty acids, sterol esters) [1]. There are a wide variety of visualisation techniques for finger-mark evidence at the disposal of forensic professionals and choice of approach relies on the type of surface (porous/non-porous), the material on which the mark has been deposited, i.e. metallic, plastic, magnetic, glass, paper and the quality of the finger-mark - age, environmental degradation, smudging. Common visualisation methods can be categorised as powder [2] [3] or chemical visualisation [4] [5]. Chemical and biological evidence may be destroyed in the case of fired ammunition relevant to forensic ballistics, spurring an interest in alternative enhancement methods for challenging samples.

Hence, a key aim of this work was to electrochemically exploit redox and conducting polymers on planar and cylindrical brass substrates for latent finger-mark enhancement. Brass is the industry standard for ammunition casings, and cartridge brass (70:30, copper to zinc ratio) [6]

Abbreviations: Abbreviation, Meaning; CA, Chronoamperometry; CE, Counter electrode; CV, Cyclic voltammetry; DPV, Differential pulse voltammetry; E, Potential; E_{app}, Applied potential; $E_p^{a/c}$, Peak potential (anodic/cathodic); EDOT, 3,4-Ethylenedioxythiophene; GCE, Glassy carbon electrode; I, Current; $I_p^{a/c}$, Peak current (anodic/cathodic); ITO, Indium tin oxide; j, Current density; NR, Neutral red; Q, Charge; RE, Reference electrode; Th, Thionine acetate; v, Scan rate; WE, Working electrode; XPS, X-ray photoelectron spectroscopy.

* Corresponding author.
E-mail address: eithne.dempsey@mu.ie (E. Dempsey).

https://doi.org/10.1016/j.forc.2025.100663
Received 15 December 2024; Received in revised form 5 March 2025; Accepted 16 April 2025
Available online 19 April 2025
2468-1709/© 2025 The Author(s). Published by Elsevier B.V. This is an open access article under the CC BY license (http://creativecommons.org/licenses/by/4.0/).

[7] is used in the making of ammunition casings. Successful latent finger-mark visualisation on metallic surfaces has been reported with varying degrees of success, requiring very high energy, long analysis times and the use of aggressive chemicals. The use of brass alloy as an electrochemical transducer presents challenges due to high reactivity, passivation, surface oxide formation and hydrogen evolution reactions [8] and can undergo dezincification, a form of selective leaching or dealloying which is the selective removal of a particular element from an alloy due to corrosion [9].

Wightman and O'Connor utilised scanning electron microscopy to develop finger-marks on brass, aluminium, and steel surfaces, common materials in ammunition casings. Employing a low thermal mass furnace, favourable results were achieved, particularly with brass samples heated to 200 °C. However, the small sample size (three donors) and the inherently destructive nature of the method, potentially leads to the loss of donor-specific information [10]. Jasuja et al. investigated the development of eccrine and sebaceous sweat generated finger-marks on metallic surfaces using an immersion approach. Favourable outcomes were observed on surfaces such as aluminium, zinc, copper, and brass. [11]. This method was further applied to fired and unfired ammunition casings by Liu et al., being successful for most unfired casings, with a limited number yielding positive results on fired cases. The study indicated that the heat and friction associated with firing had a detrimental impact on finger-marks. Liu et al. further proposed that the visualisation of finger-marks improves with longer deposition times on cases, allowing for increased corrosion. These findings shed light on the challenges posed by fired brass cases in finger-mark development and emphasise the importance of deposition duration in achieving optimal visualisation [12].

Corrosion effects have been exploited and Bond reported a series of works involving conducting powder deposited onto a latent finger-mark on a brass surface and ammunition casings requiring application of a high potential difference 1.4 kV [13] and 2.5 kV [14] [15] [16]. There are fewer reports of methodologies for latent finger-mark visualisation based on electrochemical deposition of optically or redox active materials. Such approaches allow the latent finger-mark to act as a mask or stencil on the surface, with the deposition of material in between the papillary lines/friction ridges of the finger-mark in turn visualising a "negative" of the mark. In a proof-of-concept study, Sapstead et al. examined this using stainless steel films with electro-oxidation of conducting copolymers (pyrrole and 3,4-ethylenedioxythiophene (EDOT)), achieving grade 2 and 3 quality finger-marks [17]. Beresford and Hillman employed polyaniline films on stainless steel plates, demonstrating effectiveness on both aged and fresh finger-marks. The study, tested with one donor, involved generating a variety of finger-marks under diverse sweat inducement times and deposition pressures. The practical utility of the method for forensic purposes was constrained, with only 40 % of the produced finger-marks being deemed usable [18]. In other work, Hillman employed polymerised EDOT (PEDOT), and the electrochromic deposition method achieved >50 % successful enhancements, with a 60 % success rate noted for samples aged 7 days [19].

More recently, Costa et al. employed PEDOT with successful groomed finger-mark visualisation on brass ammunition casings via a chronocoulometric method [20] while Broncová et al. electrochemically deposited poly(neutral red) with visualisation on unfired casings [21]. Hermochova et al. subsequently compared polyphenazine dyes neutral red and toluidine blue as contrasting agents for visualisation of sebaceous finger-marks (groomed) on unfired calibre cartridges [22].

Degradation of a latent finger-mark is a key issue for forensic professionals, as the ammunition casings are rarely analysed directly after use in real cases. Multiple factors such as time, humidity, heat and secondary contamination can hinder standard methods of visualisation [23]. The role of temperature is key, as heat generated from the discharge of a firearm depends on many factors e.g. type of ammunition used (single, double or triple base), the diameter of the barrel of the firearm and how many repeated firing events were performed. Many studies have reported the challenges of low recovery rates for finger-mark enhancement on cartridge casings using current forensic techniques [24] [25] [26]. Girelli et al. compared enhancement techniques based on powdering, cyanoacrylate fuming, fluorescent dying and use of acidified hydrogen peroxide on fired and unfired cartridge casings in a time study (14 days) and via thermal treatment at 200 °C. [27] The author's conclusion recommended combined use of cyanoacrylate followed by gun blue followed by Basic Yellow 40 dyeing.

The work presented here is informed by best practise guidelines for the evaluation of new finger-mark detection methods (International Fingerprint Research Group (IFRG)) [28], representing a Phase 1 pilot study of a new approach. Such research can add to continuous development of techniques that improve the prospects of recovering usable finger-mark evidence [28]. The overall aim was to produce a rapid, low energy, non-hazardous visualisation method with spatial control (lateral and vertical) using accessible chemical reagent combinations of redox and conducting polymers in a comparative study. The predominant use of groomed finger-marks (both sebaceous and eccrine) was key in ensuring deposition consistency (force and contact time) across samples during optimisation. Subsequent inclusion of a small number of natural donor finger-marks (according to pilot study [28] guidelines) provided exploratory studies on challenging brass substrates via an aging study (up to 16 months). Based on current literature, our results represent the longest aged latent finger-mark study (both groomed and natural) successfully visualised by electrochemical means.

Throughout this research, enhancement using the background electrolyte was employed for baseline/control purposes. Cross comparative studies utilised an *in-house* synthesised magnetite nanoparticle (*Magna*) brush visualisation as a reference method in lieu of the hazardous and specialist use of cyanoacrylate fuming, being more suitable for paper/plastic substrates. Mild electrodeposition conditions in a bespoke electrochemical cell were employed to achieve the highest possible score for donated (natural) finger-marks (grade-3 and level 3 (>50 %)) on brass sheets. Experimental parameters were refined, and samples subjected to extremes of temperature, culminating in visualisation of high-fidelity finger-marks on ammunition casings to the extent of potential donor identification. The work paves the way for a non-destructive, alternative to existing visualisation approaches with added advantages of long-term retention of finger-mark integrity. To our knowledge, this is the first use of electrochemical deposition of such phenothiazine *co*-polymer combinations to forensically interrogate groomed finger-marks on brass and ammunition casings.

2. Materials and methods

2.1. Reagents

Brass (CZ108/CW508L) sheets were obtained from Farnell Ltd. UK in 100 × 250 mm sized sheets. Sodium nitrate ($NaNO_3$) was purchased from VWR chemicals (www.ie.vwr.com), thionine acetate (Th) and neutral red (NR) were purchased from ThermoFisher Scientific (www.thermofisher.com) while 3,4-ethylenedioxythiophene (EDOT) was purchased from Flurochem. All compounds required no further purification. Ethanol (anhydrous ≥99.5 %) was obtained from Sigma Aldrich (www.sigmaaldrich.com) and all deionised water was obtained from the lab Millipore Milli-Q water system with a Progard® TS2 filter attached. Electrode polishing solution was a 1 μm monocrystallin diamond suspension (Akasel www.akasel.com). Brass ammunition casings were donated from a private collection, with headstamp of "*HXP 85*" indicating their manufacturing origin from the Greek Powder and Cartridge Company in 1985. These samples were fired previously, and the subsequent polishing method detailed below effectively replenished the surface to an "unfired" state; however, any stress imposed on the substrate from the act of firing was expected to be retained. For the chemical precipitation of magnetic nanoparticles, iron(III) chloride hexahydrate (97–102 %, Alfa Aesar (www.thermofisher.com)), iron(II) chloride

tetrahydrate (≥ 99 %, Fluka) and ammonium hydroxide (25 % solution in water, Acros organics (www.thermofisher.com)) were employed.

2.2. Instrumentation and software

All electrochemical experiments were carried out using a Solartron Potentiostat Model 1285 operated by Scribner Associates Corrware software package with data analysis using CorrView Version 2.3a and a CHI Electrochemical workstation model (660E) operated by CHI software (version 19.10) with Microsoft excel 365 software package and Origin Pro 2023b for data analysis. Reflectance probe and spectrophotometer was an Ocean Insight (brand of Ocean Optics BV) USB650 miniature spectrometer. Reflectance microscopy was performed using an Olympus BX51M with ColorView soft imaging system. A platinum mesh (square area 1.32 cm^2) was used for the counter electrode and a standard Ag|AgCl electrode (internal solution 3 M KCl) was employed as the reference electrode. A HUAWEI P20 lite mobile phone, running EMUI version 9.1.0 in addition with a LED desk lamp were used for photography. X-Ray Photoelectron spectroscopy was performed with a Kratos AXIS 165 instrument at the Bernal Institute, University of Limerick, Ireland. Heat degradation experiments were carried out using a Gallenkamp, size 2, muffle furnace. A bespoke electrochemical cell was fabricated with chemical resistant PET material and a Teflon inlet tube, containing copper wire (d = 1 mm) with the attachment point manipulated into a corkscrew spiral (d = 5 mm), allowing for an ammunition casing to be screwed into the connection to act as a working electrode, sealed to a watertight finish with Araldite 2-part epoxy adhesive.

2.3. Procedures

2.3.1. Preparation of monomer solutions

To ensure homogeneous solutions of the monomers, once the correct amount of compound was measured out (see Table 1 for concentrations used) it was transferred to the flask with the minimal volume of solvent. Sufficient solvent was added to the flask to fill ca. quarter of the total volume. This was then sonicated for 10 min, placed in the fridge for 5 min and then sonicated for an additional 10 min. The solution was then brought up to the mark of the vessel and was allowed to stir for 30 min. The solutions were stored in the fridge at 4 °C and stirred at room temperature for 5 min before use.

2.3.2. Ultraviolet / visible spectroscopy

The instrument was blanked with a dried surface of interest (e.g. ITO//Brass) which was cycled in the electrolyte only, using the same parameters used for film formations. Immediately following preparation, film samples were gently dried with a jet of compressed air, post formation, and placed on a level surface. In a dark room, the reflectance probe was lowered as close to the surface as possible without making contact. Room temperature (ex situ) readings were taken at three different locations with an average of 4 scans at each location. Data was analysed and 2nd derivative was calculated using OriginPro2023.

Table 1
Composition of the solutions (monomers and concentrations) used in this work for visualisation of latent finger-marks, made up in 0.1 M $NaNO_3$.

Monomer → Solution # ↓	EDOT (2 mM)	Thionine acetate (1 mM)	Neutral red (1 mM)
1	✓	–	–
2	–	✓	–
3	–	–	✓
4	✓	–	✓
5	✓	✓	–
6	–	✓	✓

2.3.3. Attenuated Total reflection infrared spectroscopy

The diamond surface was cleaned with methanol-dampened lint free tissue and allowed to dry for 5 min prior to use. The instrument was blanked to the environmental conditions of the room and background data of the clean surface of interest was obtained for background subtraction using OriginPro2023. Sample data was obtained with an average of 16 scans.

2.3.4. X-ray photoelectron spectroscopy

Samples of brass sheets were prepared via potential sweeping over the range − 0.2 to 0.5 V at 50 $mV.s^{-1}$ for 3 cycles in separate solutions of 0.1 M $NaNO_3$, 1 mM thionine acetate in 0.1 M $NaNO_3$ and 1 mM thionine acetate with 2 mM EDOT in 0.1 M $NaNO_3$.

2.3.5. Transducer preparation and cleaning

Brass strips of size 2.5 × 7 cm were cut and an exposed working area of 2.5 × 2.5 cm (6.25 cm^2) was formed on one side of the sheet with the use of insulating tape. The brass sheets were replenished with polishing, using a small amount of Brasso© (isopropyl alcohol 3–5 %, ammonia 5–10 %, silica powder 15–20 % and oxalic acid 0–3 %) applied to a rough cloth. The sheet was then brought to a lustre finish with 1 μm diamond suspension and a polishing pad. The strips were rinsed with deionised water and sonicated in ethanol for 10 min followed by drying via compressed air.

As ammunition casings were significantly different in shape, a drill was used to rotate the casing on p1200 grit polishing paper with Brasso as lubricant. The casing was then further rotated on a cloth with Brasso and finally on a fine polishing pad with 1 μm diamond suspension to bring it to a mirror finish. The working area was defined via insulating tape to give 7.07 cm^2.

In the case of the use of indium tin oxide (ITO) electrodes, they were gently wiped clean with a piece of lint free tissue, dampened with deionised water, ethanol and finally acetone. The electrode was further sonicated in ethanol for 10 min and dried via a jet of compressed air. The working area was defined via insulating tape to give an area of 6.25 cm^2.

2.3.6. Synthesis of magnetic nanoparticles and preparation of "magna brush" as benchmarking technique

Magnetic powder, acting as the bristles of the brush consists of magnetite iron particles (Fe_3O_4) may be applied using a wand with a small magnet located at the tip [2]. Chemical coprecipitation of magnetic nanoparticles was achieved based on the method by Ristic et al [29]. This involved dissolving $FeCl_3.6H_2O$ (5.833 g) and $FeCl_2.4H_2O$ (2.149 g) in 100 mL of DI water, followed by stirring under N_2 gas, while heating to 72 °C. This was followed by addition of 10 mL of 25 % ammonium hydroxide. The magnetic particles precipitated instantaneously, and the mixture was further stirred at 72 °C for a further 20 min and then allowed to cool to room temperature. The particles were allowed to settle in the solution (aided by neodymium magnets of grade N35), decanted and washed with water three times, followed by three ethanol rinses. This process was repeated until the supernatant was clear with a final ethanol wash. The particles were collected and allowed to dry in an oven at 80 °C for 3 h followed by suspension in ethanol at 1 mg. mL^{-1}.

2.3.7. Finger-mark generation

Groomed Sebaceous: The donor's hands were initially washed with soap and warm water. The finger, which was intended to provide the finger-mark, was then rubbed across sebaceous oil rich areas (forehead, down the side of the nose and behind the ear). The finger was then rubbed two to three times on the forearm, to remove any excess oils or skin cells and then gently placed on the surface of interest (1–2 s). See **Supplementary Information SI(1,2)** for scheme reflecting this process and for digitised image of finger-mark employed for groomed prints in this work. In the case of application of finger-marks to ammunition casings, the ammunition casing was cleaned as described above, then

attached to the corkscrew adaptor. Once in place, the latent finger-mark was applied in a pinch, i.e. two prints were applied (the index finger and thumb) one on the side closest to the reference electrode and one on the side of the counter electrode.

Groomed Eccrine: The hands were initially washed with soap and warm water. The cleaned hand was then doubled gloved for a minimum of thirty minutes while performing light activity. The gloves were removed, and a finger was then gently placed on the surface of interest (1–2 s).

Natural Donor: Natural donor marks were obtained randomly whereby the donor's finger was gently placed on the surface of interest (1–2 s), resulting in a representative individual finger-mark. Donors were then asked to supply a groomed finger-mark as per the method above for comparison purposes.

2.3.8. Influence of heat degradation and aging on finger-mark visualisation

Using a Gallenkamp, size 2, Muffle Furnace, temperature was set and allowed to stabilise over the course of 1–3 h. Finger-marks were applied in the same manner as that described for either the sebaceous or eccrine mark procedures. The sample was then placed into the chamber and a timer was commenced once the door was closed. Once the required time was complete, the sample was removed and allowed to cool. To examine the effect of room temperature long term aging on the print quality, both natural finger-marks and groomed sebaceous finger-marks were collected from various donors on flat brass surfaces. These finger-marks were stored in a cool dry place away from direct light (no temperature/humidity control) followed by testing at both 5 months and 16-months.

2.3.9. Scoring of visualised finger-marks

Scoring of the finger-marks in this work employed two scales. The first of these was based on the level features (one to three) present, with minute details of level three features being a key focus. While the most common level used for identification purposes is level two, robust level three information infers successful visualisation of the lower levels. Observation of "high definition" visualisation within the ridges indicates a strong enhancement method, thus allowing for loss in definition (in real casework) while retaining level two features for identification purposes. An assignment of level features in the finger-marks employed throughout this work helped establish the comparative performance of the method(s) proposed, with the assumption that prior levels are readily observed. A threshold of 50 % was employed e.g. Level 3 (>50 %) indicates that the visualised finger-mark resulted in these features over greater than 50 % of the visualised area.

Secondly, as a standard comparison to other visualisation techniques, the University of Lausanne (UNIL) [28] scale (grades 0–3) was implemented as it also focuses on level details (see Table 2 for grades and definitions).

2.3.10. Finger-mark photography

Finger-mark photographs were taken using a phone camera (**Supplementary information SI(3))** maintaining a consistent photography process. Colour manipulation was employed to create images of higher clarity, by changing brightness, temperature, contrast, and saturation levels of the image. No image manipulation such as filling in blank spaces with assumed features or merging multiple images to create a composite finger-mark was employed.

Table 2
Definitions of grades used in the University of Lausanne (UNIL) finger-mark visualisation system.

Grade	Definition
0	No ridge, no finger-mark visible
1	Ridges are visible over a small area (or over the whole mark), but it is extremely difficult to retrieve level 2 characteristics (such as minutiae) because of extremely poor ridge details.
2	Ridges are visible on almost the whole mark; level 2 characteristics can be retrieved. Nevertheless, the quality is not optimal because of a low contrast, strong background staining, or faint ridges.
3	Ridges are very well defined on the whole mark. Level 2 characteristics can easily be retrieved. The contrast is optimal with no (or extremely faint) background staining

2.3.11. Electrochemical methods

Cyclic voltammetry was performed over the potential range − 0.2 to 0.5 *V* vs Ag|AgCl (3 M KCl) at 50 $mV.s^{-1}$, while constant potential techniques involved E_{app} = 0.1, 0.25 and 0.5 V under different time or maximum charge parameters. A bespoke electrochemical cell was fabricated for visualisation techniques on the ammunition casings **(Supplementary information SI(4)).** This allowed the ammunition casing to act as the working electrode, within the 3-electrode cell.

3. Results and discussion

3.1. Screening of co-monomers feedstocks for Visualisation effectiveness

3.1.1. Redox and optical behaviour at indium tin oxide electrodes

To establish the redox behaviour of the proposed monomers and their combinations, electrodeposition was performed by potential cycling at indium tin oxide (ITO) planar electrodes and typical results for the EDOT-NR and EDOT-Th mixtures are presented in Fig. 1. In the case of the former, an initial anodic response was observed at 1 *V*, which decreased as cycling progressed. The voltammogram displayed a redox couple with anodic (oxidation) E_p^a = 0.28 V and cathodic (reduction) E_p^c = 0.008 V which may be identified as the central phenazine ring of the NR. The scan rate study (**Fig. 1 [B]**) resulted in a similar response to that obtained using neutral red alone, with more uniform increase in current density, perhaps due to the PEDOT deposition. In the case of EDOT-Th (Fig. 1 **[C]**) an initial oxidation response appeared at −0.046 *V* in cycle 1, accompanied by reduction responses at 0.065 and − 0.11 V. A second anodic response emerged at 0.17 V from cycle 3 onwards, while the cathodic responses increased upon cycling.

Both non-faradaic and faradaic characteristics of PEDOT and thionine respectively were observed via the scan rate study (Fig. 1 **[D]**) with a redox couple of E_p^a = 0.19 V and E_p^c = −0.2 V evident, superimposed on the conducting polymer background signal current. Plots of current density (*j*) vs scan rate (ν) **Fig. 1 [E]**) resulted in a linear trend and slope (m) of the log *j* vs log *v* plots were on average 0.71, being closer to a diffusion-controlled relationship (expected m = 0.5) [30] reflecting charge compensating counterion diffusion limitation within the films formed. In order to decouple the conducting and redox polymer behaviour, the voltammetric deposition and influence of scan rate on the so-formed films for individual EDOT monomer and thionine acetate deposition (under identical conditions, ITO) are shown in **Supplementary Information (SI(5)).** The influence of pH on the peak positions of thionine films has been considered in the literature and redox positions were reproducible under the conditions employed here (post deposition electrolyte pH ~6.5, unbuffered). More detailed insights into the proton coupled electron transfer processes of thionine films were the subject of a prior study in our group (EDOT-Th films at glassy carbon electrodes) [31] [32].

The composition of the electrodeposited film was investigated ex situ, under ambient room conditions using UV–vis and attenuated total reflectance infrared spectroscopy. Each form of spectral analysis was performed on a freshly formed film, immediately following formation and subsequent drying. Second derivative UV/Vis absorbance spectroscopy was also performed on all formed films at an ITO surface (Fig. 2 **[A]**). Signals for Th and NR containing films at 300 and 325 nm were attributed to a N═C chromophore. Th showed a response at 573 nm representing the blue colour of the film, and NR absorbed at 446 nm (red/orange colour). While the dominant response within the NR-Th film was attributed to NR and thus a phenazine core, 2nd derivative

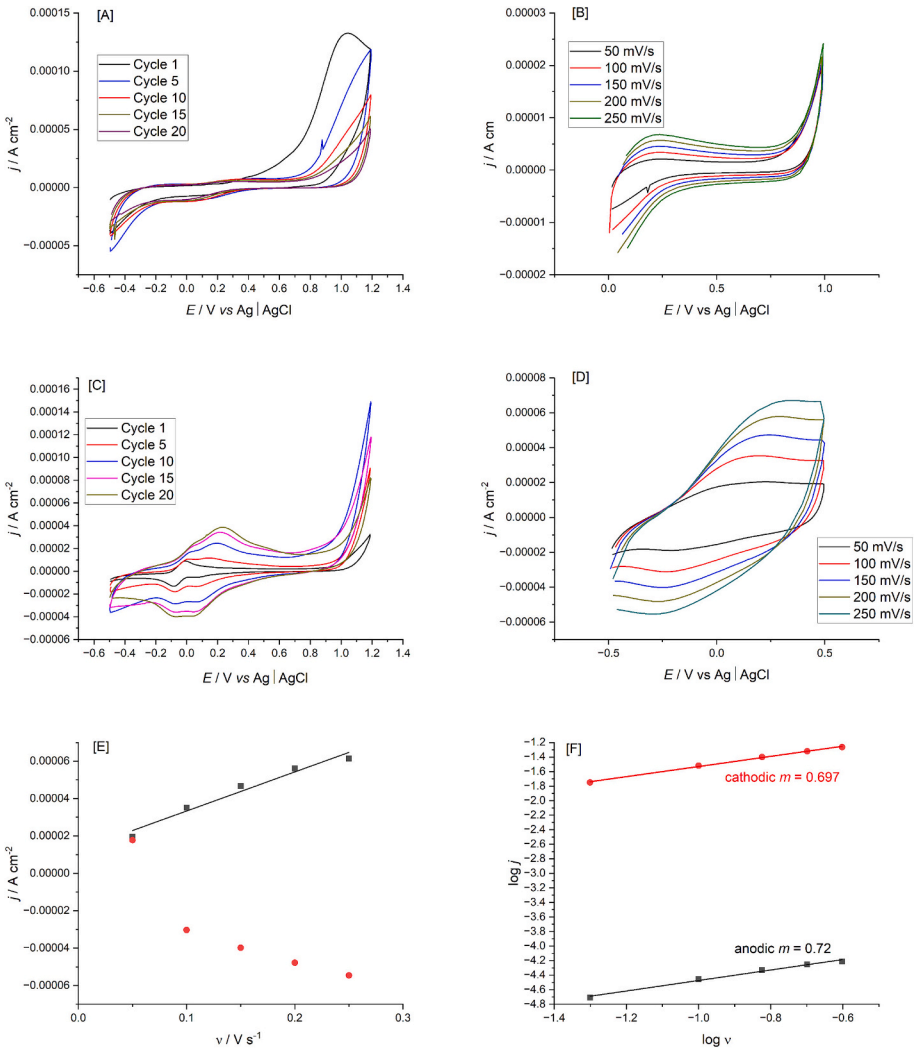

Fig. 1. [A] Cyclic voltammograms of an ITO electrode in A) 2 mM EDOT & 1 mM neutral red in 0.1 M $NaNO_3$ over the potential range − 0.5 to 1.2 *V* vs. Ag|AgCl at 100 mV.s^{-1} showing cycles 1, 5, 10, 15 & 20 (typical trace) and [B] scan rate study of the film formed in (A) in 0.1 M $NaNO_3$ over the potential range 0 to 1 V vs. Ag|AgCl. at 50, 100, 150, 200 & 250 mV.s^{-1} (typical trace). (C) Cyclic voltammograms of an ITO electrode in 2 mM EDOT & 1 mM thionine acetate in 0.1 M $NaNO_3$ over the potential range − 0.5 to 1.2 V vs. Ag|AgCl at 100 mV.s^{-1} showing cycles 1, 5, 10, 15 & 20 (typical trace) and [D] scan rate study of the film formed in [C] in 0.1 M $NaNO_3$ over the potential range − 0.5 to 0.5 V vs. Ag|AgCl at 50, 100, 150, 200 & 250 mV.s^{-1} (typical trace). [E] Plot of I_p^c vs scan rate. [F] Plot of log *j* vs log scan rate. (For interpretation of the references to colour in this figure legend, the reader is referred to the web version of this article.)

spectroscopy allowed for the observation of a shoulder (circled) which corresponded with the wavelength of Th, further indicating the presence of each within the overall polymer. IR spectroscopy was performed on the films deposited on an ITO surface as shown in Fig. 2 **[B]** **.** With the exception of the film containing NR alone, a characteristic three peak response at about 3850, 3735 and 3620 cm^{-1} was observed in all other spectra with varying degrees of intensity. The reasons behind this response may be a N—H which has been red shifted due to hydrogen bonding, or it may arise due to O—H. As the response was present in the PEDOT film alone, the presence of O—H may be more likely. In a comparative sense, the PEDOT-NR film appears to contain spectral features for both the individual monomers, while Th dominates the responses for the Th containing films. The signals at 3000–2800 (stretching of N—H of amine salts) were present in all films with the exception of NR and NR-PEDOT films and there was overlap attributed to C—H stretching of aromatic ring hydrogen atoms in this region [33]. Peaks at 1608 or 1616 cm^{-1} are associated with -NH_2 in plane deformation and a possible coupling of the N atom of the primary amine on the phenothiazine ring may cause a change in intensity and wavenumber of this peak [33].

A comparative reflectance probe measurement was also performed on films formed at a glassy carbon electrode (**Supplementary information SI(6)**)) where there was more evidence of the characteristic PEDOT optical properties (2nd derivative UV–vis spectra). Matched peaks were evident for PEDOT-Th at 220, 416, 471, 498, 525 and 558 nm with wavelengths between 400 and 600 nm being representative of PEDOT in a neutral state [34] [35]. The strong reference wavelength of 520 nm for thionine acetate [36] was observed in the Th film (518 nm). *V*ariations in the deposit formed, conjugation effects or a change in delocalisation could produce bathochromic shifts, such as those observed here [37].

3.1.2. Electrochemical characterisation of Phenazine, phenothiazine and EDOT combinations at a Brass surface

Voltammograms obtained during deposition of (co)monomers onto a brass surface (Fig. 3) did not show significant differences relative to supporting electrolyte alone. The voltammogram for 2 mM EDOT in 0.1 M $NaNO_3$ was of a similar shape to that obtained in the electrolyte alone, with passivation occurring on the initial anodic sweep from −0.2 to 0.19 *V* and a steady increase in current density until the maximum of 0.5 V was reached. A crossover was observed at 0.070 V which increased to 0.13 V in subsequent cycles. The similarities between voltammograms

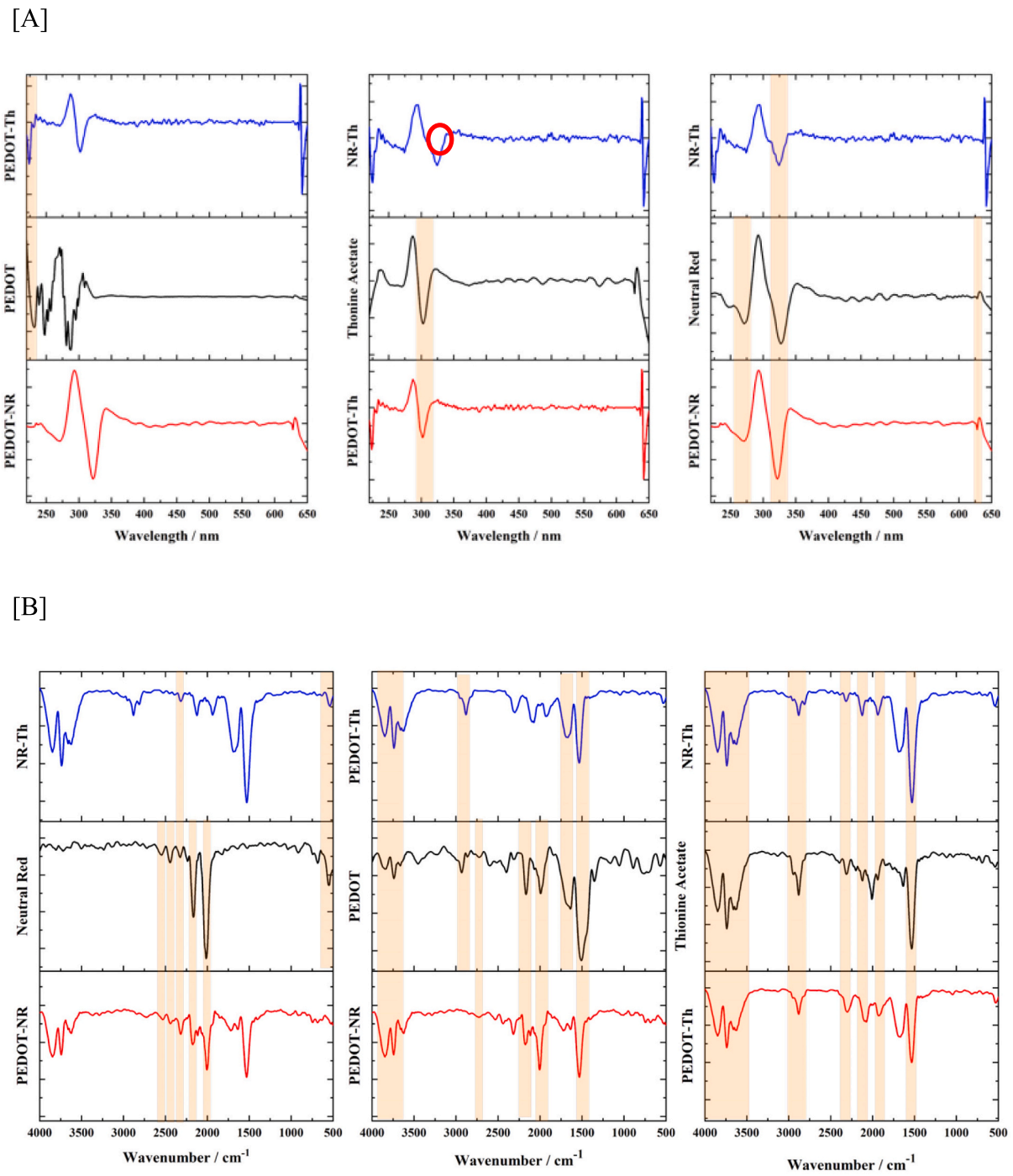

Fig. 2. [A] UV/Vis absorbance spectra (ex situ) for PEDOT containing films, thionine acetate containing films and neutral red containing films at an ITO surface. [B] IR Spectra of Neutral Red containing films PEDOT containing films and thionine containing films formed at an ITO surface by cycling at 50 mV s^{-1} over the potential range − 0.2 to 0.5 V for 20 cycles ending at −0.2.V vs Ag|AgCl (3 M KCl). (For interpretation of the references to colour in this figure legend, the reader is referred to the web version of this article.)

suggests that electrochemical measurement (at least cyclic voltammetry) was not a discernible technique for comparing the electrochemistry of the various monomer with this brass alloy as the working electrode. Some differences included the crossover potential (cycle 1) and Table 3 summarises these data with the EDOT-Th combination resulting in the most anodic shift in both crossover potential and onset potential relative to background electrolyte.

Reflectance spectroscopy (Fig. 4 **[A]**) was employed to examine the optical properties of the films formed at brass substrates. Signals associated with NR dominate in the reflectance spectra for mixed films, with those at 261, 318, 351 and 577 nm and 236, 261, 318 and 352 nm being attributed to its presence in the EDOT-NR and NR-Th films respectively. The presence of Th was attributed to one signal at 243 nm in the NR mixture and two signals at 312 and 318 nm in the EDOT mixture. IR spectroscopy at the brass surface (Fig. 4 **[B]**) provided insights into film spectral features and PEDOT-NR and NR-Th films produced similar spectra with the main peaks observed at 2030, 2120 and 2200 cm^{-1} indicative of the phenazine ring structures. Similar peaks were observed in the case of NR alone at 1990, 2100 and 2210 cm^{-1}, while for PEDOT and Th individual films, a characteristic peak for C═O was observed at

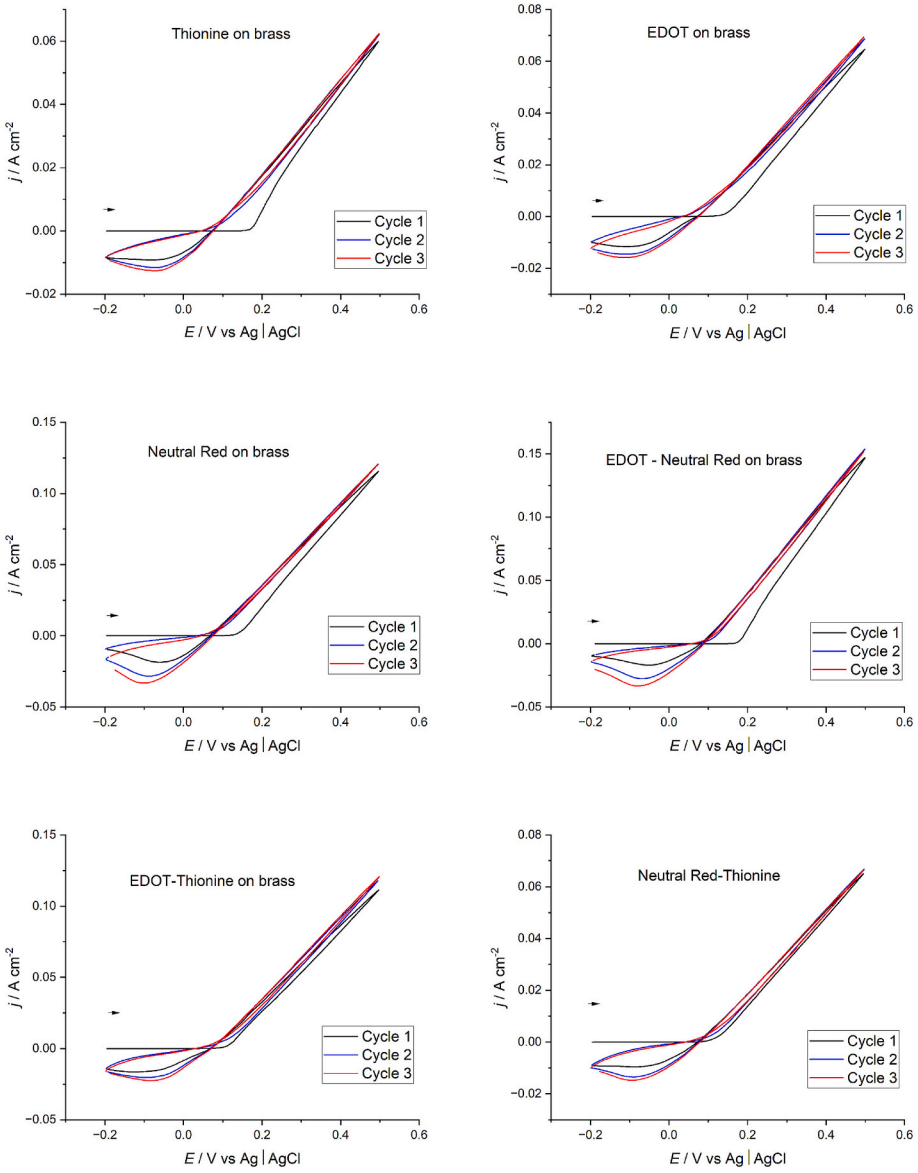

Fig. 3. Cyclic voltammograms of 2 mM EDOT, 1 mM Th, 1 mM NR, 2 mM EDOT & 1 mM NR, 2 mM EDOT & 1 mM Th and 1 mM NR & 1 M Th in 0.1 M $NaNO_3$ at a brass surface over the potential range − 0.2 to 0.5 V vs. Ag|AgCl at 100 m*V*.s^{-1} (typical traces throughout).

Table 3
Crossover and breakdown potentials observed in cycle 1 at a planar brass surface.

Solution	Crossover potential / V	Onset potential / V
$NaNO_3$	0.075	0.164
EDOT	0.079	0.199
Thionine acetate	0.080	0.129
Neutral red	0.066	0.141
EDOT-NR	0.074	0.179
EDOT-Th	0.063	0.099
NR-Th	0.072	0.142

1701 cm^{-1}, along with an indicative peak for N—O at 1531 cm^{-1} which may occur as a result of NO_3^- ions in the electrolyte.

3.2. Cyclic Voltammetric methods for finger-mark visualisation

Electrodeposition studies were performed on freshly cut brass sheets, which underwent an initial cleaning step (ethanol rinse and jet of compressed air). Upon potential cycling, voltammograms did not indicate any uniquely identifiable redox features, with the distinctive shape being attributed to the electrochemical properties of brass [38], while the addition of a latent finger-mark did not alter this in any of the solutions tested. *V*isualisation of a groomed finger-mark was performed in triplicate, via cyclic voltammetry over the potential range − 0.2 to 0.5 V at 50 mV.s^{-1} for 3 cycles in each solution and mixture. Fig. 5 presents each of the visualised finger-marks prepared under the same electrochemical conditions using each monomer composition examined (see Table 1.) High contrast black and white images with the respective test (visualisation) solution are presented.

Level 3 features were commonly found across the visualisation methods, with a consistent minimum grade 2 visualisation up to grade 3. All formulations tested produced reproducible visualisations, with an average level 3 (<50 %) for the EDOT-NR and NR-Th mixtures while EDOT-Th resulted in an average level 3 (>50 %). EDOT-Th resulted in the highest likelihood of achieving level 3 features, while NR-Th resulted in the most variation in levels obtained. Reference methods showed poor success rates and included powder methods (I) talcum and (II) chemically prepared magnetite (*in house* Magna brush (see

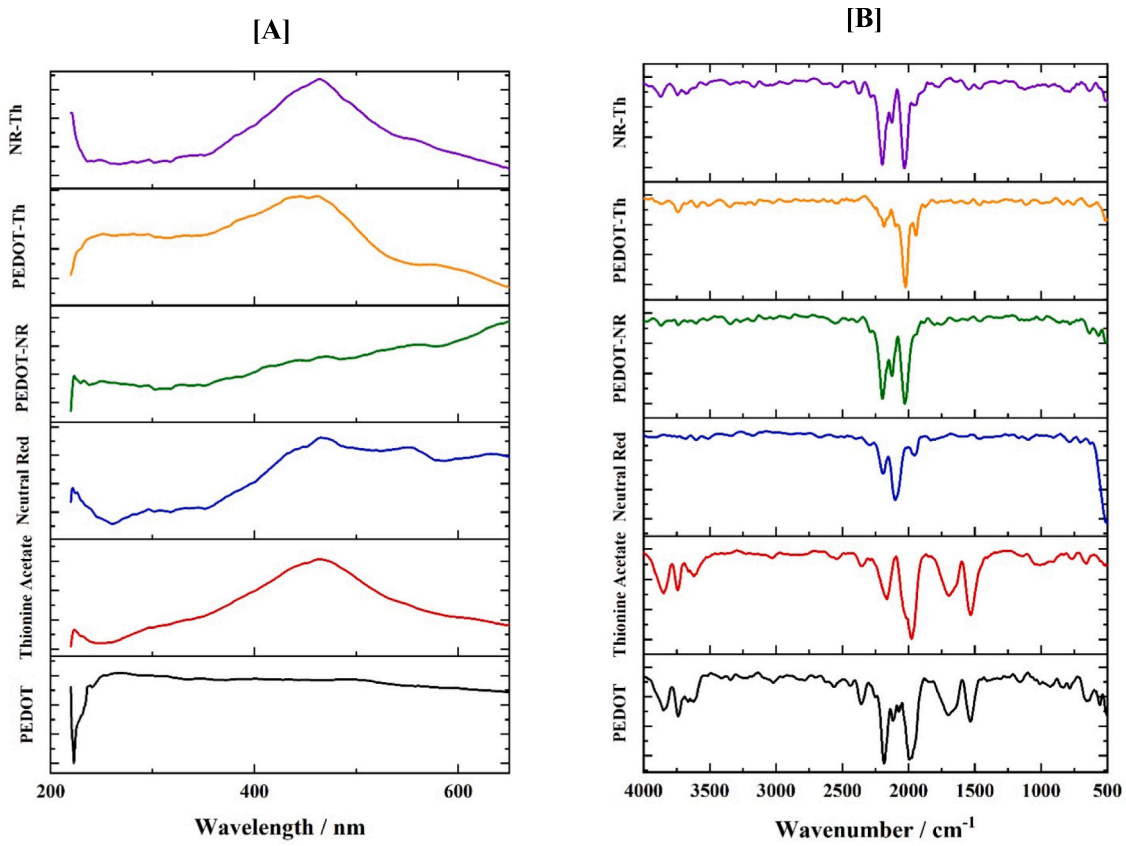

Fig. 4. [A] Reflectance spectra of films formed at a brass surface. [B] IR spectra of the electrodeposited films on a brass surface.

Supplementary Information SI(7)). There were no identifiable level 3 features for both methods and resulted in a grade of 0 to 1, as a finger-mark is visible but no discerning ridges were present, for (I) and grade of 1 to 2 in the case of (II).

The use of reflectance microscopy followed, observing the core at a magnification of x1000. In Fig. 6 each of these cores are shown, with 4 visible ridges, if counting 1–4 left to right (Fig. 6 [A]). Ridges 1 and 2 are connected and would be classified as the exact core of the finger-mark, containing 5–6 pores across in total. Ridge 3 was a ridge ending containing a single pore just at the end of the ridge and ridge 4 continues the overall finger-mark pattern containing a possible 2–3 pores down its length. EDOT visualisation (Fig. 6 **[A]**) at x1000 magnification produced highly textured ridges (diameter ca. 450 μm) with a mixture of deposited material (dark area) and protected surface (light area) across the ridge. Pores were somewhat visible but did not appear to have definitive shapes and there was "bleed" into the ridges. This also appeared to affect the ridge edges with ridge 3 and 4 appearing to be connected, removing the ridge ending characteristic from ridge 3. Th visualisation (Fig. 6 **[B]**), interestingly, appeared to have increased the sizes of the pores within the ridges, almost appearing as corridors within the ridges (ridge diameter ca. 450 μm, pore diameter ca. 150 μm). This could easily be mistaken for additional ridges if the endings or connection points were not visible at this location. This may be the reason why level 3 features were so prominent within this visualisation technique when photographed with a standard camera. Definition of the ridge edges was successful and while the area between the ridges was small (approximately 50–100 μm), the contrast between protected metal surface (light area) and deposited material (dark area) was large enough to define the boundaries.

In the case of NR (Fig. 6 **[C]**) visualisation at this magnification appeared to generate ridge detail at a fine level, while the boundary of the ridge to the metal surface appeared rough or textured, the shape or curvature of the ridge was still visible. EDOT-NR (Fig. 6 **[D])** produced a visualised mark which in some cases was difficult to see. Ridge details with defined boundaries were visible, however, it appeared that the pores within the ridges break the ridge, creating lagoon-like structures, making characterisation of the ridge shape difficult. EDOT-Th (Fig. 6 **[E])** produced the best quality visualisation of the ridges with crisp ridge boundaries and defined ridge and pore shape throughout the core. The fine details observed in this visualisation begs the question whether one of the pores on ridge 1 was actually a ridge break, which was not observed with the other methods and whether there was a small lake feature on ridge 4, previously thought to be a pore. NR-Th (Fig. 6 **[F])** also produced ridges of fine detail like that produced with NR alone with some apparent smudging of the ridges.

To further understand the processes which were taking place at the brass surface during visualisation, the elemental regions of Cu, Zn and O were examined using XPS following potential sweeping of the brass sheet in 0.1 M $NaNO_3$ for 3 cycles at 100 mV s^{-1} with comparison to untreated brass sheets (Fig. 7). Starting with the copper region, a clear difference in peak area was observed (**Supplementary Information SI (8)**) indicating the higher copper signals at the surface of the treated brass, strengthening the view that the dezincification process was playing a role in the surface composition. Cu^0 in a $2p_{3/2}$ state increased from 1.3 % to 9.8 % surface composition while Cu^{2+} within CuO increased from 0.8 % to 4 %. The increase of both elemental copper and the oxide suggested the redeposition of the metal and oxidation of some material during the experiment. In relation to zinc surface composition (**Supplementary Information SI(9)**), the relative peak areas suggest a drop in the zinc concentration at the surface. There was relatively no change in how the zinc was bound within the surface matrix and it appeared that there was no redeposition or additional surface activity with zinc, other than its removal. In terms of oxygen, the most evident difference was the oxide signal, which increased from 3.1 % to 11.3 %,

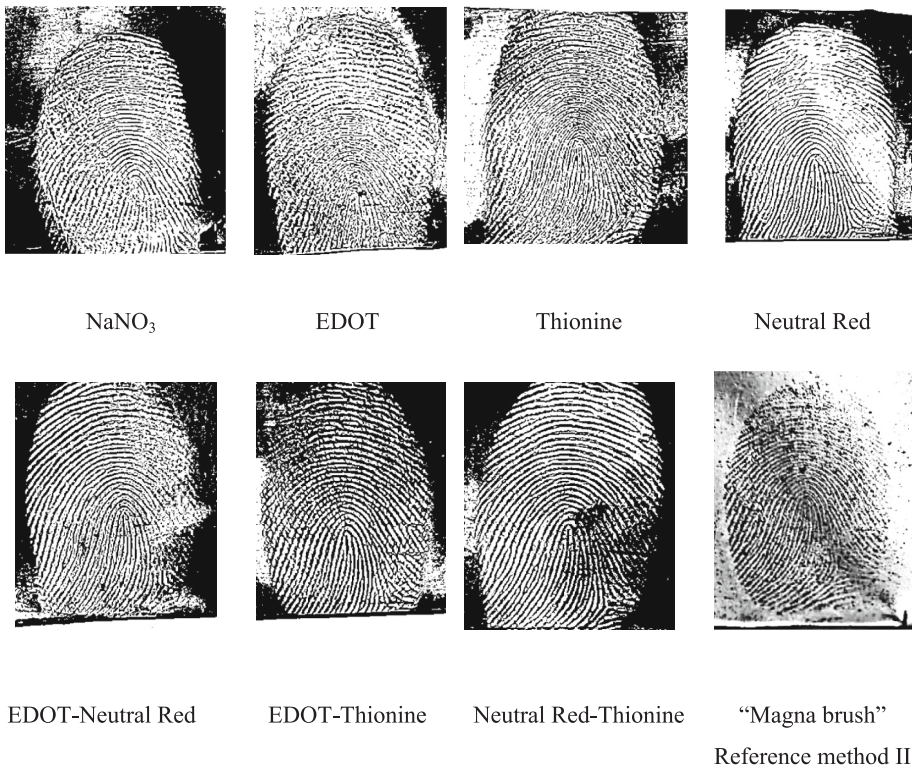

Fig. 5. High contrast images of groomed latent finger-marks visualised at a brass sheet via cyclic voltammetry over the potential range − 0.2 to 0.5 V vs. Ag|AgCl at 50 mV.s^{-1} for 3 cycles in the solutions identified in Table 1, with background electrolyte solution of 0.1 M $NaNO_3$, and subsequent monomer solutions in 0.1 M $NaNO_3$ to include 2 mM EDOT, 1 mM thionine acetate and 1 mM neutral red (separate monomers) and mixtures of EDOT-NR, EDOT-Th, NR-Th together with non-electrochemical visualisation of a latent finger-mark with a magna brush as a control (Reference method II). (For interpretation of the references to colour in this figure legend, the reader is referred to the web version of this article.)

matching the trend observed with the increase of the copper oxide post analysis. Table 4 below summarises the findings.

To explore the composition of the materials deposited at the brass surface during the visualisation process, XPS was employed using brass sheet samples modified electrochemically with both Th and EDOT-Th solutions. Deposition was performed via the previously used cyclic voltammetric method over the range of −0.2 to 0.5 *V* at 50 mV.s^{-1} for 3 cycles. The binding energies of nitrogen were observed (Fig. 7) with both Th and EDOT-Th showing two nitrogen signals at 398.4 and 399.8 eV, with the lower being representative of the C═N of a phenazine ring and the upper of a N—C, possibly of aromatic nature [39] such as the amine groups attached to the ring structure of the phenothiazine core of thionine. Both monomers of interest contain the sulfur atom, but a variation was observed and the lower binding energies achieved indicated possibilities of both copper and zinc interactions (see Table 5 for matched data). Most notable was the variation in the copper persistence at the surface when Th alone was deposited. The brass dezincification process results in an increase in copper concentrations at the brass surface due to its removal and subsequent redeposition [40] [41]. Free copper cations were present in solution which, during the visualisation process (cyclic voltammetry) may allow Cu—S bonds to form [40].

3.3. Potentiostatic methods for finger-mark visualisation

While successful visualisation was achieved with the potentiodynamic approach above, a simplified method of visualisation would appeal more to forensic professionals, which in turn would require less complex instrumentation. Hence, a potentiostatic method with fixed applied voltage $E_{app} = 0.5$ V was examined using a brass surface, without a latent finger-mark, which was held in solutions of $NaNO_3$, Th and EDOT-Th until charges of 1, 5 and 10C were passed (see chronocoulometry (Fig. 8) and associated data **(Supplementary Information SI(10)).**

Deposition of materials up to a charge of 1C resulted in a mild colour change on the surface, which was easily removed, while passage of 10C resulted in a deep colour change on the surface, with increase of texture and removable material which may hinder visualisation of a latent finger-mark. It was concluded that films formed upon passage of 5C resulted in the most successful deposition of material, with minimal damage to the brass surface. In order to further fine tune the deposition parameters, films formed via 4, 5 and 6C were examined with relevant reflectance microscopy images shown in Fig. 9. When visualised in the Th solution, following the passing of 4C the detail between the ridges appeared with a purple/blue hue and the pores within the ridges appeared to “bleed” into each other, almost making it appear as if the ridges were hollow channels. In the case of 5C films the ridge detail showed a much more defined distance between the ridges, however, there was a loss of some definition in the pore shapes along the ridges. Passage of 6C produced a highly textured surface, and definition between the ridges was very clear, however, pore features along the ridges were not observed. The mixture of EDOT-Th using 4C resulted in finger-marks which were successfully defined, with a blue hue observed between the ridges with excellent definition between the ridges, including indicative pores, while also introducing a red hue across the defined ridge detail. The implementation of 6C films produced ridges from which the general shape of the detail could be obtained, however, clear definition between the ridges was not visible. Overall, the use of 5C for deposition was the most successful combined with the use of EDOT-Th resulting in the clearest visualisation of the ridge detail and the presence of pores which would be deemed successful for individual matching purposes.

3.3.1. Visualisation of aged natural donor finger-marks

To lower the energy requirements for the method further, an applied

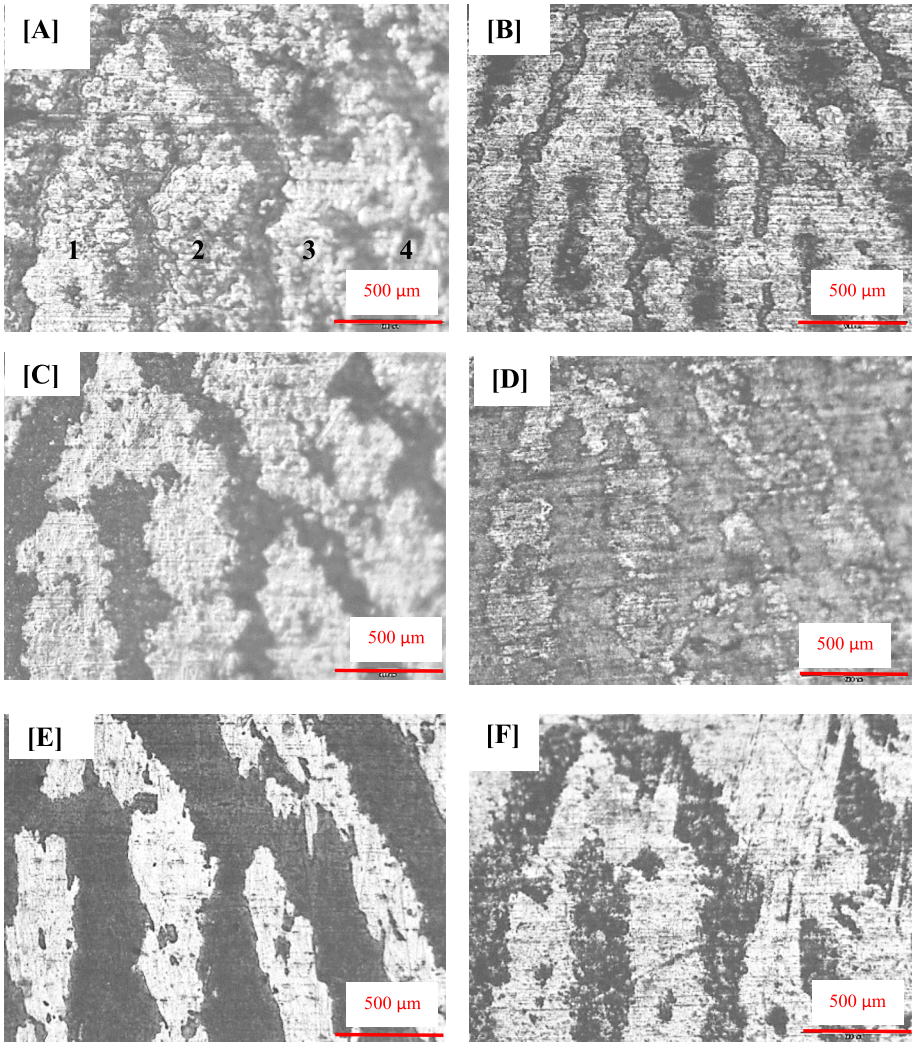

Fig. 6. Microscope images (x 1000) of finger-mark cores visualised at a brass sheet via cyclic voltammetry over the potential range − 0.2 to 0.5 *V* vs. Ag|Ag at 50 mV. s^{-1} for 3 cycles in 0.1 M $NaNO_3$ containing the monomers A) EDOT, B) Th, C) NR and the mixed monomer solutions of D) EDOT-NR, E) EDOT-Th and F) NR-Th.

potential of 0.1 *V* was employed for $t = 60$ and 120 s and seconds, in order to evaluate whether gaseous production at the counter electrode diminished (with associated risk of bubble adsorption) while simultaneously achieving successful visualisation of a latent finger-mark. Under $E_{app} = 0.1$ V ($t = 60$ s), minimal visualisation occurred, prompting an increase to 120 s, resulting in clearly defined ridge details and observable grades of 2 and 3 (Fig. 10[A]). Two of the factors which may hinder brass visualisation methods are the age of the latent finger-mark on the surface, and the potential degradation of the sample due to the heat experienced during the discharge of the firearm. The time passed between the "event" and the analysis is a major contributing factor to the efficacy of analytical methods as natural degradation, contamination, dilution and destruction of evidence are all more likely. Here, latent finger-marks were applied to brass surfaces and stored at room temperature in a dark and dry place with testing at 5 and 16 months. Finger-marks were supplied by eight donors with two samples obtained from each donor, a "natural" finger-mark and a subsequent groomed finger-mark. These finger-marks were obtained from both male and female donors, as it was found that female finger-marks were more difficult to visualise than males, possibly due in part to size differences and subsequent increase in ridge density compared to male hands [46]. Finger-marks stored for 5 months were applied via a split print method, and in total 8 donors submitted marks which were then visualised via the optimum potentiostatic method of $E_{app} = 0.1$ *V* for 120 s in EDOT-Th mixed solution (see Fig. 10[B])).

Using the EDOT-Th mixed solution, grade 2 was most commonly achieved, with some instances of grade 3 and identifiable level 3 (<50 %) features, across the obtained the eight donor samples while electrolyte alone achieved a maximum grade 2. Fig. 10[C,D] shows natural and groomed prints visualised with the EDOT-Th solution following a 16-month storage period. Aged latent finger-marks were successfully visualised both in the groomed and natural forms from male and female donors with grade 2 observed in all cases, with indicative level 3 (<50 %) features observed in the natural male finger-mark and groomed female finger-mark. Comparatively, at the 16-month time point, the visualisation performed in $NaNO_3$ alone did not produce any prints with level 3 features, with a single instance of unsuccessful visualisation (see **Supplementary Information SI(10)** for Tabulated data).

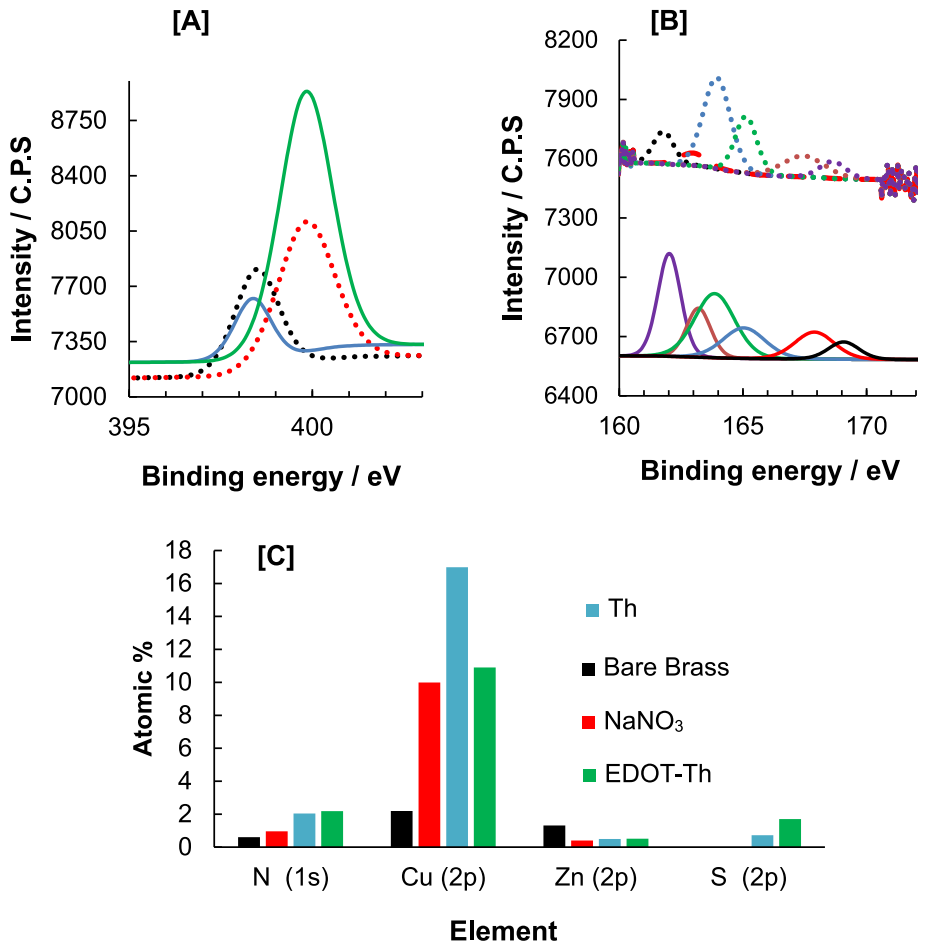

Fig. 7. XPS graphs from brass surface which underwent cyclic voltammetry over the potential range − 0.2 to 0.5 *V* vs. Ag|AgCl at 50 mV.s^{-1} for 3 cycles in 0.1 M $NaNO_3$ with (solid lines) EDOT-Th or (dashed lines) Th, showing the binding energies of A) Nitrogen B) Sulphur and C) histogram showing the elemental % atomic quantification at surface for untreated brass (black), and brass surface which underwent cyclic voltammetry over the potential range − 0.2 to 0.5 V vs. Ag|AgCl at 50 mV.s^{-1} for 3 cycles in 0.1 M $NaNO_3$ (red), Th (purple) and EDOT-Th (green). (For interpretation of the references to colour in this figure legend, the reader is referred to the web version of this article.)

Table 4
Averaged total percentage of elements at the surfaces of brass samples.

	O 1 s	C 1 s	N 1 s	Cu 2p	Zn 2P
Untreated Brass	25.9	69.7	0.9	2.2	1.3
$NaNO_3$ cycled Brass	28.4	63.7	1	6.2	0.8

*Brass was cycled in 0.1 M $NaNO_3$ over the potential range of −0.2 to 0.5 *V* at 100 mV.s^{-1}, untreated brass was within the same solution, however, protected from the solution via insulation tape.

Table 5
Identity of sulphur binding energies found with Th and EDOT-Th deposition layers on a brass surface.

Binding energy	Spectral line	Identity
161.8	$2p_{3/2}$	Sulfide – CuS [42]
161.9	$2p_{3/2}$	Sulfide – ZnS [43]
162.0	$2p_{3/2}$	Sulfide – CuS [44]
163.1	$2p_{1/2}$	$CuFeS_2$ [45]

The time allotted for "aged" finger-marks on brass vary a great deal in the literature, with successful visualisation reported via electrostatic adsorption of finger-marks on ammunition casings which were 10 days old [47], cyanoacrylate fuming for natural and groomed prints which were 2 weeks old [48] and silver electroless deposition on 6-week-old

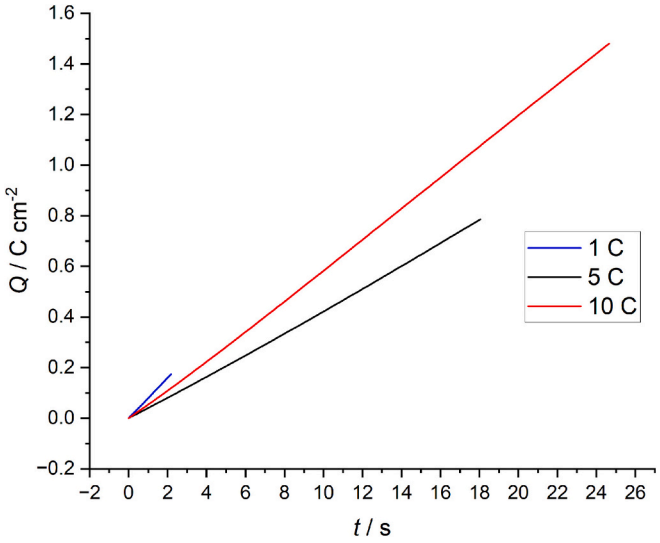

Fig. 8. Charge density vs. time plot for brass sheets held at E_{app} = 0.5 V in 1 mM thionine acetate with 0.1 M $NaNO_3$ until 1 (blue), 5 (black) and 10 (red) C was passed. (For interpretation of the references to colour in this figure legend, the reader is referred to the web version of this article.)

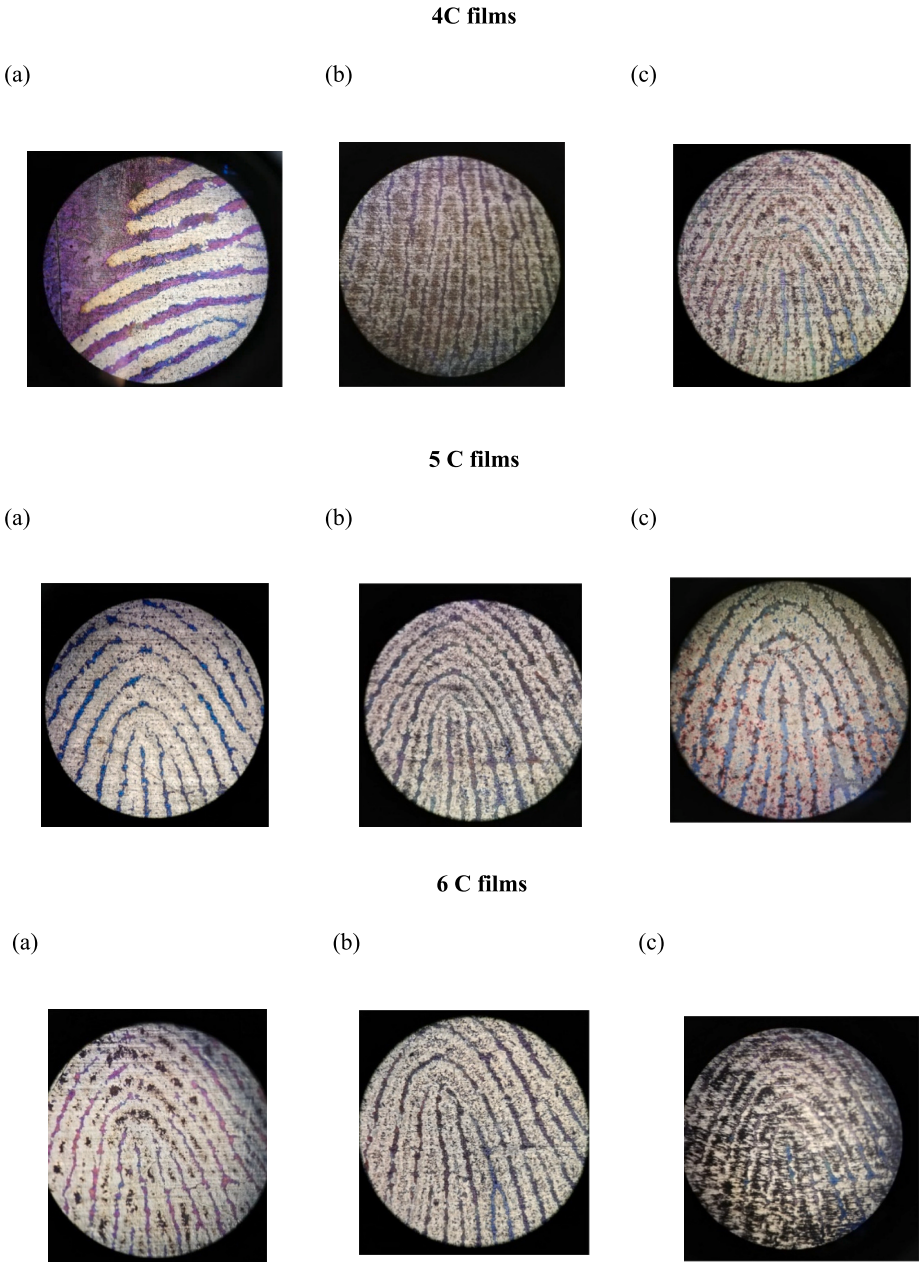

Fig. 9. Images of ridge details of a visualised latent finger-mark x100 magnification visualised upon application of $E_{app} = 0.5\ V$ in three test solutions (a) 0.1 M $NaNO_3$, (b) 1 mM thionine acetate and (c) 2 mM EDOT with 1 mM thionine acetate until a charge of 4C, 5C and or 6C charge was reached.

finger-marks [49]. Lam et al. reported successful visualisation on a 22-week-old latent finger-mark on ammunition casings via disulfur dinitride fuming [50]. Using electrochemical methods, Costa et al. reported successful finger-mark visualisation up to 30 days for sebaceous marks and 15 days for eccrine marks using a constant potential method [20]. To our knowledge, our results demonstrate some of the longest aged latent finger-marks (both groomed and natural) visualised by electrochemical means when compared with current literature.

3.3.2. *Visualisation of heat-treated finger-marks*

While the heat generated from the discharge of a firearm varies significantly depending on size and power of the firearm used, studies

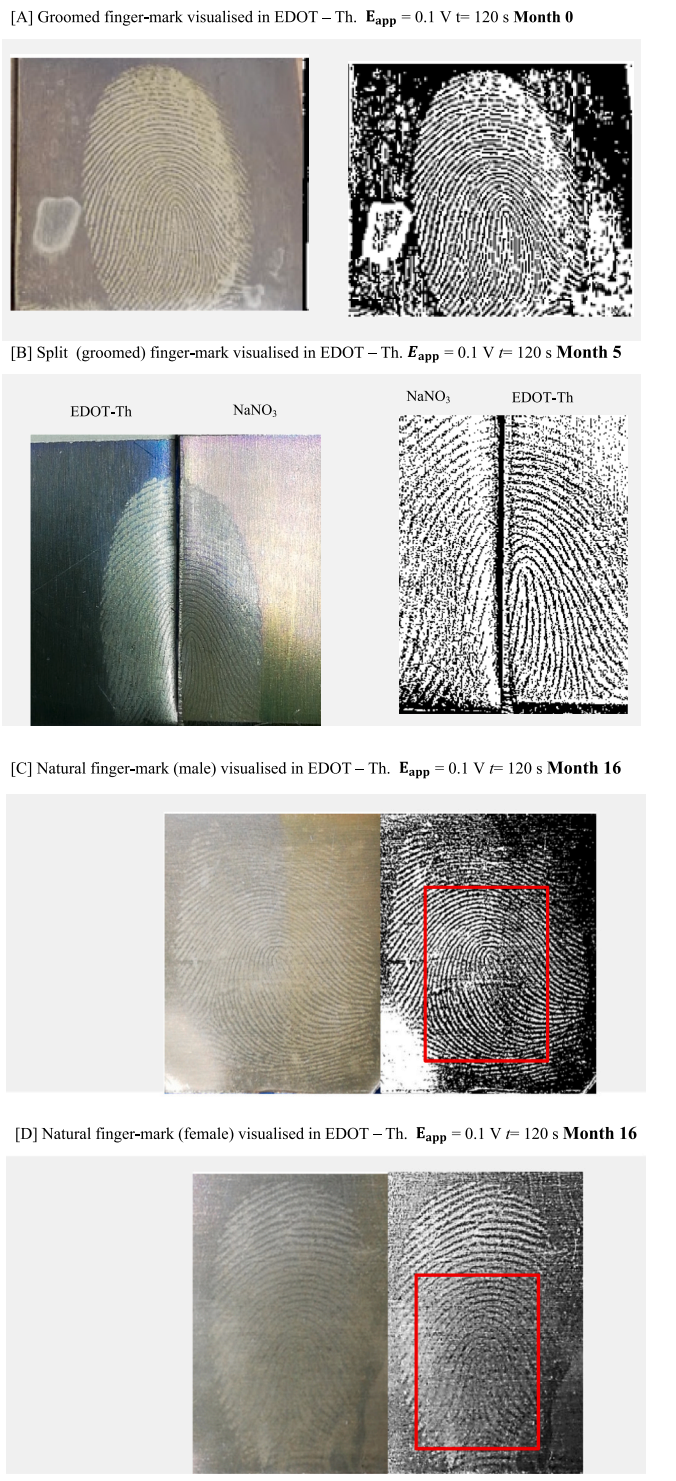

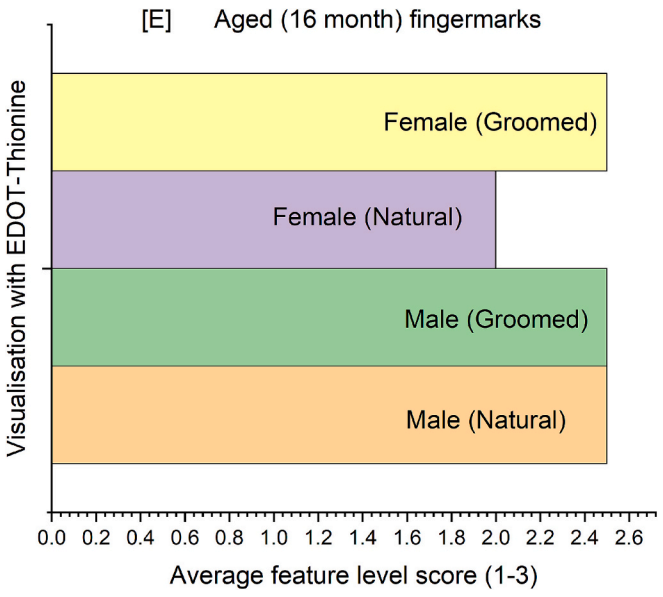

Fig. 10. [A] Photograph and high contrast image of latent finger-mark on a brass surface visualised in 2 mM EDOT and 1 mM thionine acetate in 0.1 M $NaNO_3$ at E_{app} = 0.1 V vs. Ag|AgCl for t = 120 s [B]: Photograph of and zoomed in high contrast image of visualised 5-month-old groomed latent finger-mark at E_{app} = 0.1 V vs. Ag|AgCl for 120 s split across two brass sheets showing left $NaNO_3$ and right EDOT-Th. Natural 16-month-old latent finger-marks on a brass surface visualised with EDOT-Th upon E_{app} = 0.1 V vs. Ag|AgCl for 120 s with [C] male and [D] female. [E] Average level of visualisation score for 16-month-old finger-marks showing both male and female donors for natural and groomed finger-marks.

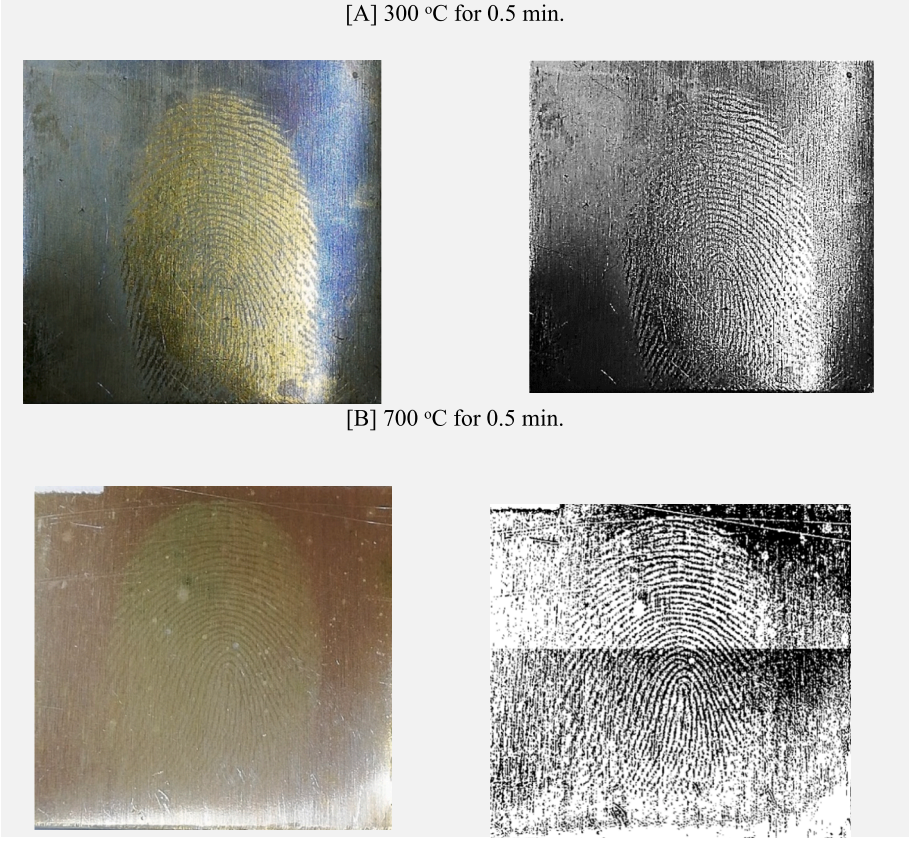

Fig. 11. Photograph and high contrast image of latent finger-mark visualised in EDOT-Th via potentiostatic method with $E_{app} = 0.1\ V$ vs. Ag|AgCl for 120 s post heating [A] 300 °C for 0.5 min [B] 700 °C for 0.5 min.

performed on small calibre firearms (which would be more likely for street level crimes), can achieve temperatures of approximately 540 °C within the bore of the firearm [51]. These temperatures could increase greatly if an automatic weapon was employed, with multiple rounds being fired in a short period of time. The initial explosion of a propellent lasts <1 ms, however, to fully stress test the latent finger-marks much greater time periods were employed in this work.

Groomed sebaceous latent finger-marks and groomed eccrine finger-marks were employed in the temperature study, for the purposes of examining the feasibility of this method post thermal treatment of brass substrates. Only the sebaceous finger-marks were successfully visualised, possibly due in part to the high-water content of eccrine sweat, with removal due to the high heat applied. Initially latent finger-marks ($n = 4$) were held at 100 °C for 25 min. This was carried out to ensure that all the water present within the finger-mark was removed. Fig. 11 **[A]** shows a visualised finger-mark, post heat treatment at 300 °C with successful visualisation obtained up to grade 2 in all samples (n = 4). The shorter time employed (0.5 min) allowed for the visualised finger-marks to regain the clear definition between the ridges. Upon exposure to 700 °C, it was evident that this visually altered the brass surface resulting in a silver colour, reflecting an annealing process. Latent finger-marks were invisible once the sample was removed from the furnace, however, potentiostatic visualisation produced visualised latent finger-marks as shown in Fig. 11 **[B]**. Finger-marks of clear level 2 features were achieved three times, while in one instance an indicative finger-mark was observed which would not even be classified as having level 1 features, as the overall shape of the finger-mark was unclear.

Temperature degradation studies of latent finger-marks have been reported in the literature in a wide variety of scenarios. Latent finger-marks on the surface of lightbulbs which were allowed reach temperatures of 156.3 °C have been successfully visualised with black powders [52]. Bleay et al. reported successful visualisation of latent finger-marks on brass via cyanoacrylate fuming with basic yellow 40 dye and gun blueing methods after reaching temperatures of 600 °C for 5 min [53]. The application of high temperatures to metal surfaces has also been investigated as a visualisation technique, using the protective nature of the latent finger-mark to hinder surface oxidation creating a contrast at the metal surface. There have also been reports of enhanced visualisation of a grade 2 (CAST System) finger-marks on a brass surface heated to 600 °C [10]. Girelli et al. performed an intensive investigation into the visualisation of latent finger-marks on ammunition casing with the mark present before firing, using brass sheets heated to 200 °C as the control, reporting successful visualisation with a cyanoacrylate, gun blueing and fluorescent dye method for groomed prints applied to both surfaces [54].

To our knowledge there are no reports in the literature of template based electrochemical methods used to develop heat degraded groomed latent finger-marks on brass surfaces and in this work, finger-marks were successfully visualised up to the temperatures expected during the firing of ammunition. It is understood that there is an inherited variability to the deposition of these finger-marks, due to numerous factors, mainly the donors. Some people are naturally better at producing latent finger-marks, or one may deposit a “better” finger-mark once and subsequently have the quality of the mark drop on subsequent depositions. However, this study is an important stepping stone towards demonstrating the potential and feasibility of this early-stage methodology with the aid of natural donor finger-marks.

3.4. *Visualisation of finger-marks on ammunition casings*

Despite the high probative value of ammunition casings, development of good contrast friction ridge impressions on these surfaces

[A]

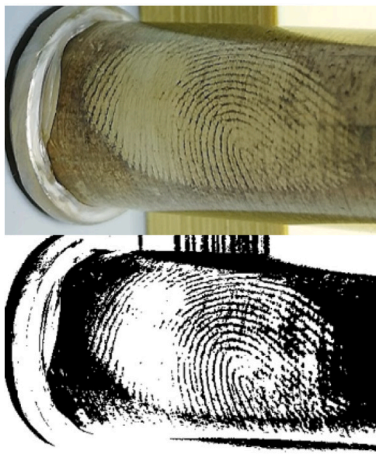

[B]

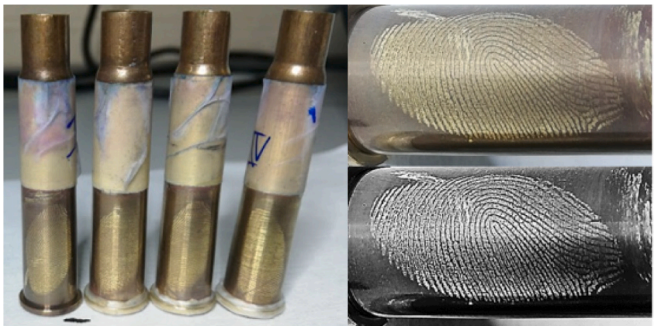

Fig. 12. [A] Photograph and high contrast image of latent finger-mark on a brass ammunition casing, visualised with E_{app} =0.1 V for 120 s in EDOT-Th [B] Visualised latent finger-mark on ammunition casing via potentiodynamic method using EDOT-Th.

remains a significant forensic challenge [24] and many studies have reported the demands of low recovery rates for finger-mark enhancement on cartridge casings using current forensic techniques [24] [25]. In the research presented thus far, potentiostatic methods were optimised for brass strips (subjected to aging and thermal treatments), to include both coulometry with optimisation of charge (5C) passed upon application of 0.5 V and subsequently application of a lower applied potential (0.1 V) for 120 s. As the composition of cartridge brass differs slightly from the CZ108/CW508L sheet brass both potentiodynamic and potentiostatic techniques were examined using the EDOT-Th co-monomer mixture.

The change in surface curvature of the substrate prompted the incorporation of additional grading vectors in the assessment of visualised finger-marks on ammunition casing surfaces. This adjustment was necessary due to the higher likelihood of smudging on the curved surface compared to the flat brass surface. In all instances regions of successful visualisation were closely linked to parallel alignment with the Pt gauze counter electrode; however, partial visualisations were achievable in some instances. The potentiostatic method with $E_{app} = 0.1$ V for 120 s was utilised for groomed latent finger-marks subsequently applied on a brass ammunition casing surface resulting in grade 2 visualisation for all prints produced ($n = 4$), **Supplementary Information SI(11).**

Overall, the low voltage, rapid potentiostatic method was successful in the visualisation of the groomed finger-marks, on ammunition casings and further improvements were made via the potentiodynamic approach. This involved sweeping over the potential range − 0.2 to 0.5 V at 50 $mV.s^{-1}$ for 6 cycles, resulting in some of the most successful groomed finger-mark enhancement on this surface, as shown in Fig. 12. This grade 3 finger-mark exhibited level 3 (>50 %) features across the entire area and pore details along the ridge structures were visible. Successful imaging and contrast were even observed with the secondary finger-mark on the casing (thumb print on opposite side of index print). Average results within replicates (n = 4) result in average Grade 3 (**Supplementary Information [SI(12)]** representing high-quality groomed finger-mark visualisation achieved relative to the higher voltage and duration approaches by Costa et al. and Bond et al. [20] [55].

This systematic study of novel and accessible polymeric materials electrodeposited on challenging brass substrates under mild and controllable parameters represents a methodology capable of resolving third level details with considerable potential for further, extended studies. Fine tuning of conditions for electrochemical deposition onto the insulating template of finger-mark friction ridges on a conducting substrate was successfully deployed using aged and thermally treated brass substrates as a representative surface with extension to ammunition cartridges.

4. Conclusions

Overall, several surface, optical and electrochemical methods were employed to systematically visualise groomed latent finger-marks on conventional planar electrode surfaces (ITO) followed by brass sheets and finally spent ammunition casings. Analysis techniques involved use of potentiodynamic and potentiostatic techniques which were complemented by film optical studies using reflectance/IR spectroscopy with reflectance microscopic analysis. Simultaneous deposition of polymeric materials coupled with dissolution of the CuZn alloy was verified with the aid of XPS surface analysis. Co-monomer feedstocks of EDOT, thionine acetate, and neutral red were compared to assess their efficacy in revealing latent finger-marks. EDOT-Th solution emerged as the most reliable, consistently realising latent finger-marks at level 3 (> 50 %) features, including the finer detail of pores within the ridges.

Significantly, to our knowledge, this strategy is the first instance of electrochemically polymerising thionine, and consequently, the EDOT-Th mixture onto on brass as an attractive methodology which employs low toxicity, accessible, water-based reagents enabling contrast optimisation and controllable film formation. In comparison to cyanoacrylate fuming and dye staining, the method is independent of the finger-mark's chemical residues required for the polymerisation of the monomer and generation of contrast.

Successful visualisation of high-resolution latent finger-marks (groomed), resulting in grade 3 and level 3 (> 50 %) features, was achieved on the surfaces of brass ammunition casings using aqueous electrochemical methods in <120 s. As an operational study, finger-marks subjected to a temperature of 700 °C were successfully visualised at level 2 features, overcoming challenges posed by brass annealing temperatures and potential structural alterations to the surface. Natural finger-marks, aged up to 16 months, were effectively visualised on brass surfaces, displaying level 3 (> 50 %) features.

This research has demonstrated a Phase 1 proof of principle investigation informed by IFRG guidelines [28] resulting in a rapid and low energy visualisation technique for latent finger-marks deposited on challenging substrates (brass surfaces and cartridge casings), requiring simple instrumentation and no sample preparation. Based on the data generated we believe this to be worthy of extension to research Phase 2 (optimisation and comparison), where testing of a larger pool of donor eccrine samples will be necessary together with comparison to established operational techniques. The progression of this non-destructive, controllable and safer (non-toxic) approach, based on successful development of identifiable friction ridge impressions also has advantages of sample retention integrity in forensic biometrics. In addition, the possibility of extension to knives, coins and other types of firearm evidence is an intriguing prospect.

CRediT authorship contribution statement

Colm McKeever: Writing – original draft, Validation, Methodology, Investigation, Formal analysis, Data curation. **Eithne Dempsey:** Writing – review & editing, Supervision, Resources, Project administration, Funding acquisition, Formal analysis.

Funding Declaration

The authors would like to acknowledge the Dept. Chemistry PhD Teaching Fellowship, Maynooth University and Irish Research Council PhD Scholarship GOIPG/2021/250 for funding this work.

Declaration of competing interest

The authors declare that they have no known competing financial interests or personal relationships that could have influenced the work reported in this paper.

Acknowledgements

XPS analysis was performed by Dr. Fattima Laffir at the Bernal Institute, University of Limerick, Ireland.

Declaration of competing interest

The authors declare that they have no known competing financial interests or personal relationships that could have appeared to influence the work reported in this paper.

Appendix A. Supplementary data

Supplementary data to this article can be found online at https://doi.org/10.1016/j.forc.2025.100663.

Data availability

Data will be made available on request.

References

[1] S. Cadd, M. Islam, P. Manson, and S. Bleay, "Fingerprint composition and aging: a literature review," Sci. Justice, vol. 55, no. 4, pp. 219–238, 2015/07/01/ 2015, doi: doi:https://doi.org/10.1016/j.scijus.2015.02.004.
[2] S.M. Bleay, Solid phase selective deposition techniques, in: Fingerprint Development Techniques, 2018, pp. 199–220.
[3] S.M. Bleay, Optical detection and enhancement techniques, in: Fingerprint Development Techniques, 2018, pp. 111–153.
[4] S.M. Bleay, Amino acid reagents, in: Fingerprint Development Techniques, 2018, pp. 221–274.
[5] S.M. Bleay, Reagents for other eccrine constituents, in: Fingerprint Development Techniques, 2018, pp. 275–282.
[6] K. Yaqoob, F. Hashmi, and W. Hassan Tanveer, "Failure analysis of cartridge brass shell," Eng. Fail. Anal., vol. 138, p. 106325, 2022/08/01/ 2022, doi: doi:https://doi.org/10.1016/j.engfailanal.2022.106325.
[7] K. Hajizadeh, M. Tajally, E. Emadoddin, and E. Borhani, "Study of texture, anisotropy and formability of cartridge brass sheets," J. Alloys Compd., vol. 588, pp. 690–696, 2014/03/05/ 2014, doi: doi:https://doi.org/10.1016/j.jallcom.2013.11.091.
[8] H.Z. José, P. Ingrid, O. Ruben, Redox Potentials as Reactivity Descriptors in Electrochemistry, in: K. Rozina (Ed.), Redox, Rijeka: IntechOpen, 2019, p. 4.
[9] Corrosion atlas, in: F. Khoshnaw, R. Gubner (Eds.), Corrosion Atlas Case Studies, Elsevier, 2022, pp. 1–46.
[10] G. Wightman and D. O'Connor, "The thermal visualisation of latent fingermarks on metallic surfaces," Forensic Sci. Int., vol. 204, no. 1, pp. 88–96, 2011/01/30/ 2011, doi: doi:https://doi.org/10.1016/j.forsciint.2010.05.007.
[11] O. P. Jasuja, G. Singh, and J. Almog, "Development of latent fingermarks by aqueous electrolytes," Forensic Sci. Int., vol. 207, no. 1, pp. 215–222, 2011/04/15/ 2011, doi: doi:https://doi.org/10.1016/j.forsciint.2010.10.011.
[12] S. Liu, M. Pflug, R. Hofstetter, M. Taylor, The effect of pH on electrolyte detection of fingermarks on cartridge cases and subsequent microscopic examination, J. Forensic Sci. 60 (1) (2015) 186–192, https://doi.org/10.1111/1556-4029.12620.
[13] J. W. Bond, "On the electrical characteristics of latent finger mark corrosion of brass," J. Phys. D. Appl. Phys., vol. 41, no. 12, p. 125502, 2008/05/23 2008, doi: https://doi.org/10.1088/0022-3727/41/12/125502.
[14] J.W. Bond, Imaging fingerprint corrosion of fired brass shell casings, Rev. Sci. Instrum. 80 (7) (2009), https://doi.org/10.1063/1.3183578.
[15] J.W. Bond, Visualization of latent fingerprint corrosion of Brass, J. Forensic Sci. 54 (5) (2009) 1034–1041, https://doi.org/10.1111/j.1556-4029.2009.01108.x.
[16] S. Sykes, J.W. Bond, "a comparison of fingerprint sweat corrosion of different alloys of brass," (in eng), J. Forensic Sci. 58 (1) (2013) 138–141, https://doi.org/10.1111/j.1556-4029.2012.02300.x.
[17] R. M. Sapstead, N. Corden, and A. Robert Hillman, "Latent fingerprint enhancement via conducting electrochromic copolymer films of pyrrole and 3,4-ethylenedioxythiophene on stainless steel," Electrochim. Acta, vol. 162, pp. 119–128, 2015/04/20/ 2015, doi: doi:https://doi.org/10.1016/j.electacta.2014.11.061.
[18] A.L. Beresford, A.R. Hillman, "electrochromic enhancement of latent fingerprints on stainless steel surfaces," (in eng), Anal. Chem. 82 (2) (2010) 483–486, https://doi.org/10.1021/ac9025434.
[19] R.M. Brown, A.R. Hillman, Electrochromic enhancement of latent fingerprints by poly(3,4-ethylenedioxythiophene), Phys. Chem. Chem. Phys. 14 (24) (2012) 8653–8661. https://doi.org/10.1039/C2CP40733G.
[20] C.V. Costa, A.M.L. Assis, J.D. Freitas, J. Tonholo, A.S. Ribeiro, A low-potential electrochemical method for fast development of latent fingerprints on brass cartridge cases by electrodeposition of poly(3,4-ethylenedioxythiophene), Nano Select 1 (4) (2020) 405–412, https://doi.org/10.1002/nano.202000040.
[21] G. Broncová, T. Slaninová, and M. Trchová, "Characterization of electrochemically visualized latent fingerprints on the steel substrates," J. Solid State Electrochem., vol. 26, no. 11, pp. 2423–2433, 2022/11/01 2022, doi: https://doi.org/10.1007/s10008-022-05245-4.
[22] S. Hermochová, P. Hlavín, M. Novotný, M. Vrňata, G. Broncová, Electrochemical visualization of latent fingerprints using polyphenazine dyes on brass cartridges, Monatshefte für Chemie - Chemical Monthly 155 (8) (2024) 851–858, https://doi.org/10.1007/s00706-024-03222-3.
[23] G. Christofidis, J. Morrissey, J.W. Birkett, Detection of fingermarks—applicability to metallic surfaces: a literature review, J. Forensic Sci. 63 (6) (2018) 1616–1627, https://doi.org/10.1111/1556-4029.13775.
[24] A. Dove, Follow-up: Fingermark Development on Fired Cartridge Cases through the Electrodeposition of Gun Blue, Journal of Forensic Identification 68 (4) (2018) 567–587.
[25] H.J. Swofford, L.S. Paul, S.M. Steffan, D. Bonar, Development of latent fingerprints on fired Brass cartridge cases: impact of latent print development using acidified hydrogen peroxide on forensic firearm and Toolmark examinations (in English), JFI 63 (4) (2013) 359–368.
[26] A.J. Dominick, K. Laing, A comparison of six fingerprint enhancement techniques for the recovery of latent fingerprints from unfired cartridge cases (in English), JFI 61 (2) (2011) 155–165.
[27] C.M.A. Girelli, B.J.M. Lobo, A.G. Cunha, J.C.C. Freitas, F.G. Emmerich, Comparison of practical techniques to develop latent fingermarks on fired and unfired cartridge cases, Forensic Science International (Online) (2015), https://doi.org/10.1016/j.forsciint.2015.02.012 suppl. C, vol. 250, pp. 17–26, 2015 May 01 2023-11-14.
[28] Guidelines for the assessment of fingermark detection techniques, (in English), *Journal of forensic identification* 64 (2) (2014) 174.
[29] M. Ristić, T. Fujii, H. Hashimoto, I. Opačak, S. Musić, A novel route in the synthesis of magnetite nanoparticles, Mater. Lett. 100 (2013) 93–97, https://doi.org/10.1016/j.matlet.2013.03.013.
[30] Z. Masood, H. Muhammad, I.A. Tahiri, "comparison of different electrochemical methodologies for electrode reactions: a case study of paracetamol," (in English), Electrochem 5 (1) (2024) 57–69, https://doi.org/10.3390/electrochem5010004.
[31] S. Warren, D. Rathod, T. McCormac, E. Dempsey, Investigations into the use of a thionine/PEDOT layer as an NADH electrocatalyst with applications in glutamate sensing, ECS Trans. 25, 28 (2010) 21–32, https://doi.org/10.1149/1.3309674 [Online]. Available, https://www.scopus.com/inward/record.uri?eid=2-s2.0-79952757084&doi=10.1149%2f1.3309674&partnerID=40&md5=3f2406b7acf20f9c44fc0c609e81d293.
[32] B. Murphy, B. Singh, A. Delaney, S. Warren, E. Dempsey, Phenothiazine Redox Active Conducting Polymer Films at Nanocomposite Surfaces, J. Electrochem. Soc. 167 (2) (2020) 027525, https://doi.org/10.1149/1945-7111/ab6a83.
[33] E. Topçu, M. Alanyalıoğlu, Electrochemical formation of poly(thionine) thin films: the effect of amine group on the polymeric film formation of phenothiazine dyes, J. Appl. Polym. Sci. 131 (1) (2014), https://doi.org/10.1002/app.39686.
[34] C. Yang, J. Yi, X. Tang, G. Zhou, Y. Zeng, "studies on the spectroscopic properties of poly(neutral red) synthesized by electropolymerization," (in English), React. Funct. Polym. 66 (11) (2006) 1336–1341, https://doi.org/10.1016/j.reactfunctpolym.2006.03.015.
[35] J. Guay, P. Kasai, A. Diaz, R. Wu, J.M. Tour, L.H. Dao, Chain-length dependence of electrochemical and electronic properties of neutral and oxidized soluble .alpha.,.alpha.-coupled thiophene oligomers, (in English), Chemistry of materials 4 (5) (1992) 1097–1105, https://doi.org/10.1021/cm00023a031.
[36] J.H.O. Owino, et al., "electrochemical Immunosensor based on Polythionine/gold nanoparticles for the determination of aflatoxin B1," (in English), Sensors (Basel, Switzerland) 8 (12) (2008) 8262–8274, https://doi.org/10.3390/s8128262.
[37] S. Hayashi, Highly crystalline and efficient red-emissive π-conjugated polymer film: tuning of macrostructure for light-emitting properties, Materials Advances 1 (4) (2020) 632–638, https://doi.org/10.1039/D0MA00218F. https://doi.org/10.1039/D0MA00218F.

[38] G. Broncová, T. Slaninová, M. Trchová, V. Prokopec, P. Matějka, T.V. Shishkanova, Optimization of electrochemical visualization of latent fingerprints with poly (neutral red) on Brass surfaces, Polymers 13 (19) (2021) 3220.
[39] R. Lachhab, M. Galai, A. Ech-chebab, R.A. Belakhmima, M.E. Touhami, I. Mansouri, Comparative study of the corrosion behavior of three alpha brass alloys used in potable water distribution equipment in aggressive soil using electrochemical measurements, Ceram. Int. 50 (3) (2024) 4282–4295, https://doi.org/10.1016/j.ceramint.2023.10.185.
[40] J. Gayathri, K. S. Selvan, and S. S. Narayanan, "A novel sensor for the determination of Hg2+ in waters based on octadentate ligand immobilized multi-walled carbon nanotube attached to paraffin wax impregnated graphite electrodes (PIGE)," J. Solid State Electrochem., vol. 22, no. 9, pp. 2879–2888, 2018/09/01 2018, doi: https://doi.org/10.1007/s10008-018-3984-1.
[41] I. Pandey, P.K. Bairagi, N. Verma, Electrochemically Grown Polymethylene Blue Nanofilm on Copper-Carbon Nanofiber Nanocomposite: An Electrochemical Sensor for Creatinine, Sensors Actuators B Chem 277 (2018) 562–570, https://doi.org/10.1016/j.snb.2018.09.036.
[42] G. Deroubaix, P. Marcus, X-ray photoelectron spectroscopy analysis of copper and zinc oxides and sulphides, Surf. Interface Anal. 18 (1) (1992) 39–46, https://doi.org/10.1002/sia.740180107.
[43] A.N. Buckley, H.J. Wouterlood, R. Woods, The surface composition of natural sphalerites under oxidative leaching conditions, Hydrometallurgy 22 (1) (1989) 39–56, https://doi.org/10.1016/0304-386X(89)90040-6.
[44] V.I. Nefedov, Y.V. Salyn, P.M. Solozhenkin, G.Y. Pulatov, X-ray photoelectron study of surface compounds formed during flotation of minerals, Surf. Interface Anal. 2 (5) (1980) 170–172, https://doi.org/10.1002/sia.740020503.
[45] Q. Yin, G. H. Kelsall, D. J. Vaughan, and K. E. R. England, "Atmospheric and electrochemical oxidation of the surface of chalcopyrite (CuFeS2)," Geochim. Cosmochim. Acta, vol. 59, no. 6, pp. 1091–1100, 1995/03/01/ 1995, doi: doi: https://doi.org/10.1016/0016-7037(95)00026-V.
[46] S. Sharma, R. Shrestha, K. Krishan, T. Kanchan, "sex estimation from fingerprint ridge density. A review of literature," (in eng), Acta Biomed 92 (5) (2021) e2021366, https://doi.org/10.23750/abm.v92i5.11471.
[47] J. Xu, Z. Zhang, X. Zheng, J.W. Bond, A modified electrostatic adsorption apparatus for latent fingerprint development on unfired cartridge cases, J. Forensic Sci. 62 (3) (2017) 776–781, https://doi.org/10.1111/1556-4029.13344.
[48] M. Pitera, V. G. Sears, S. M. Bleay, and S. Park, "Fingermark visualisation on metal surfaces: an initial investigation of the influence of surface condition on process effectiveness," Sci. Justice, vol. 58, no. 5, pp. 372–383, 2018/09/01/ 2018, doi: doi:https://doi.org/10.1016/j.scijus.2018.05.005.
[49] I.C. Payne, I. McCarthy, M.J. Almond, J.V. Baum, J.W. Bond, The effect of light exposure on the degradation of latent fingerprints on Brass surfaces: the use of silver Electroless deposition as a visualization technique, J. Forensic Sci. 59 (5) (2014) 1368–1371, https://doi.org/10.1111/1556-4029.12524.
[50] R. Lam, D. Hockey, J. Williamson, and N. G. R. Hearns, "Latent fingermark development on fired and unfired brass ammunition under controlled and blind conditions," Forensic Sci. Int., vol. 337, p. 111369, 2022/08/01/ 2022, doi: doi: https://doi.org/10.1016/j.forsciint.2022.111369.
[51] Characterization of Bore Temperatures and Stresses in Small Caliber Gun Barrels, 2019.
[52] O. Colella, M. Miller, E. Boone, S. Buffington-Lester, F.J. Curran, T. Simmons, The effect of time and temperature on the persistence and quality of latent fingerprints recovered from 60-watt incandescent light bulbs (in English), J. Forensic Sci. 65 (1) (2020) 90–96, https://doi.org/10.1111/1556-4029.14133.
[53] S. M. Bleay, P. F. Kelly, R. S. P. King, and S. G. Thorngate, "A comparative evaluation of the disulfur dinitride process for the visualisation of fingermarks on metal surfaces," Sci. Justice, vol. 59, no. 6, pp. 606–621, 2019/11/01/ 2019, doi: doi:https://doi.org/10.1016/j.scijus.2019.06.011.
[54] C.M.A. Girelli, M.A. Vieira, K. Singh, A.G. Cunha, J.C.C. Freitas, F.G. Emmerich, "recovery of latent fingermarks from brass cartridge cases: evaluation of developers, analysis of surfaces and internal ballistic effects," (in eng), Forensic Sci. Int. 290 (2018) 258–278, https://doi.org/10.1016/j.forsciint.2018.07.026.
[55] J.W. Bond, C. Heidel, Visualization of latent fingerprint corrosion on a discharged Brass Shell casing, J. Forensic Sci. 54 (4) (2009) 892–894, https://doi.org/10.1111/j.1556-4029.2009.01059.x.